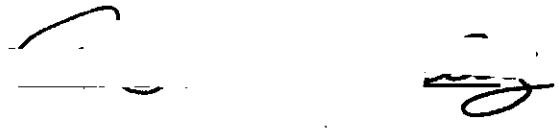


In presenting the dissertation as a partial fulfillment of the requirements for an advanced degree from the Georgia Institute of Technology, I agree that the Library of the Institute shall make it available for inspection and circulation in accordance with its regulations governing materials of this type. I agree that permission to copy from, or to publish from, this dissertation may be granted by the professor under whose direction it was written, or, in his absence, by the Dean of the Graduate Division when such copying or publication is solely for scholarly purposes and does not involve potential financial gain. It is understood that any copying from, or publication of, this dissertation which involves potential financial gain will not be allowed without written permission.

A handwritten signature in dark ink, appearing to be 'R. J. ...', is located below the main text block.

7/25/68

THE EFFECT OF IONIC COLLISIONS ON
THE INTERNAL ENERGY OF DIATOMIC MOLECULES

A THESIS

Presented to
The Faculty of the Graduate Division
by
Philip Charles Cosby

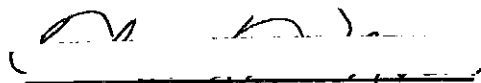
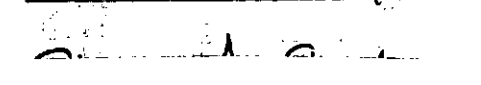


In Partial Fulfillment
of the Requirements for the Degree
Master of Science in Chemistry

Georgia Institute of Technology

June, 1969

THE EFFECT OF IONIC COLLISIONS ON
THE INTERNAL ENERGY OF DIATOMIC MOLECULES

Approved:

Date approved by Chairman: June 2, 1969

ACKNOWLEDGMENTS

It is with sincere appreciation that I acknowledge the invaluable and understanding assistance of my research advisor, Dr. Thomas F. Moran, in the construction of the apparatus, acquisition and interpretation of the data, and in the preparation of this manuscript. I am also grateful to Dr. Earl W. McDaniel and Dr. Sidney L. Gordon for reading the thesis.

A major portion of the apparatus used in this work was built by my fellow graduate students F. C. Petty, D. C. Fullerton, and A. F. Hedrick. I would like to express my appreciation to Mr. M. E. Rucker whose machining of a majority of the hardware significantly accounted for the performance of the instrument and to Mr. G. E. O'Brien for the construction of the electronics necessary for its operation.

This research has been supported by a grant from the National Aeronautics and Space Administration. A Summer Teaching Traineeship from the National Science Foundation in 1968 is gratefully acknowledged.

TABLE OF CONTENTS

	Page
ACKNOWLEDGMENTS	ii
LIST OF TABLES	v
LIST OF ILLUSTRATIONS	vi
SUMMARY	viii
CHAPTER	
I. INTRODUCTION	1
General	
Experimental Method	
Review of Previous Research	
II. APPARATUS	7
Introduction	
Ion Source and Optics	
Nier Mass Spectrometer	
Retarding Lens System	
Collision Chamber	
127° Electrostatic Sector	
Residual Gas Analyser System	
Vacuum System	
Sample Gas System	
III. KINEMATICS OF THE COLLISION	29
IV. EXPERIMENTAL PROCEDURES AND RESULTS	40
General	
Rotational Excitation	
Vibrational Excitation	
V. COMPARISON WITH THEORY	56
Introduction	
Classical Calculation	
Comparison of Results	

TABLE OF CONTENTS (Continued)

CHAPTER	Page
VI. CONCLUSIONS	73
APPENDIX	75
LITERATURE CITED	77

LIST OF TABLES

Table	Page
1. Typical Potentials in the Source and Acceleration Lens System	13
2. Typical Voltages on the Retarding Lens System	17
3. Comparison of Calculated Values of ΔV_{sector} with Observed Values for Various Kinetic Energies of He^+	25
4. Calculation of Observables for the Excitation of the $J = 0 \rightarrow J = 2$ Rotational Transition of $X \sum_g^+ D_2$ by 12.20 eV LAB (Ar^{40+}) at Different Laboratory Angles of Detection	39
5. Relative Populations of the Lower Rotational Levels of D_2 at 300°K	46
6. Relative Transition Probabilities Normalized to the Sum of the Transition Probabilities Observed at a Given Velocity	49

LIST OF ILLUSTRATIONS

Figure	Page
1. Functional Overall View of Experimental Apparatus	8
2. Schematic View of Ion Source (Front); Filament Cap Removed	10
3. Schematic View of Ion Source (Top); Filament Supports Removed	11
4. Schematic View of Retarding Lens System (Top)	16
5. 127° Electrostatic Velocity Selector	20
6. Schematic Representation of Collision in LAB System . . .	32
7. Schematic Momentum Vector Diagram for Arbitrary Collision Showing Initial and Final Coordinates of Scattered Ion in LAB and CM Systems	34
8. Schematic Momentum Vector Diagram for both Elastic and Inelastic Collisions Showing Initial and Final Coordinates of Scattered Ion in LAB and CM Systems	36
9. Velocity Spectrum of 12.90 eV LAB Ar^+ in System $\text{Ar}^+ + \text{D}_2$	42
10. Rotational Spectrum of D_2 Resulting from Collisional Excitation by 12.90 eV LAB Ar^+	43
11. Variation in Relative Rotational Transition Probabilities with Relative Velocity in System $\text{Ar}^+ + \text{D}_2$	47
12. Energy Loss Spectrum of 9.9 eV LAB O^+ in System $\text{O}^+ + \text{O}_2$	51
13. Energy Loss Spectrum of 14.6 eV LAB O^+ in System $\text{O}^+ + \text{O}_2$	52
14. Energy Loss Spectrum of 20.0 eV LAB O^+ in System $\text{O}^+ + \text{O}_2$	53

LIST OF ILLUSTRATIONS (Continued)

Figure		Page
15.	Energy Loss Spectrum of 15.6 eV LAB N_2^+ in System $N_2^+ + N_2$	55
16.	Variation with L of Vibrational Transition Probabilities Calculated from Equations (45) and (56) for the System $O^+ + O_2$	64
17.	Variation with L of Vibrational Transition Probabilities Calculated from Equations (45) and (63) for the System $O^+ + O_2$	66
18.	Probability of the Transition $v = 0 \rightarrow 1$ in the System $O^+ + O_2$ Compared to that Predicted by Equations (45) and (63). $L = 0.600 \text{ \AA}$	67
19.	Probability of the Transition $v = 0 \rightarrow 2$ in the System $O^+ + O_2$ Compared to that Predicted by Equations (45) and (63). $L = 0.600 \text{ \AA}$	68
20.	Probability of the Transition $v = 0 \rightarrow 3$ in the System $O^+ + O_2$ Compared to that Predicted by Equations (45) and (63). $L = 0.600 \text{ \AA}$	69

SUMMARY

Relative differential inelastic cross sections for specific rotational and vibrational transitions of diatomic molecules due to collisional excitation have been measured in the laboratory energy region of 10-20 eV using a beam apparatus.

A mass selected ion beam is decelerated to low kinetic energies in a retarding lens system and focused onto a neutral target gas in a rotatable collision chamber. The velocity distribution of the inelastically scattered ions is scanned by a 127° cylindrical electrostatic velocity selector. Ions passed by the velocity selector are then mass analysed by a quadrupole mass spectrometer and detected. Internal excitation of the target molecules appears as discrete energy losses in the velocity spectrum of the scattered ions.

Relative differential inelastic cross sections for the collisional excitation of rotational transitions have been measured in the systems $\text{Ar}^+ + \text{D}_2$, $\text{O}_2^+ + \text{D}_2$, and $\text{N}_2^+ + \text{H}_2$. Only transitions corresponding to $\Delta J = +2$ have been observed. An upper limit for higher rotational transitions has been set at less than three per cent those for which $\Delta J = +2$. The velocity dependence of the relative differential cross sections for the transitions $J = 0 \rightarrow 2, 1 \rightarrow 3, 2 \rightarrow 4, 3 \rightarrow 5, 4 \rightarrow 6$ has been studied in detail for the system $\text{Ar}^+ + \text{D}_2$ in the relative velocity region of $7.12 - 9.05 \times 10^5$ cm/sec. The absolute differential inelastic cross section for the $J = 0 \rightarrow 2$ transition in D_2 is estimated to be 0.15 ± 0.10 Å²/sr.

Relative differential inelastic cross sections for the collisional excitation of specific vibrational transitions in the systems $O^+ + O_2$ and $N_2^+ + N_2$ have been measured. Transitions for which the change in the vibrational quantum number is unity are found to predominate at low energies. As the relative energy of the collision is increased, however, multiquantum transitions become dominant. Simultaneous vibrational excitation of both the ion and the target molecule is observed in the system $N_2^+ + N_2$.

The relative vibrational transition probabilities measured for the system $O^+ + O_2$ are compared with those predicted by the approximate quantum-mechanical theory developed by Edward H. Kerner and C. E. Treanor for the collinear collision of a particle with a harmonic oscillator using an exponential interaction potential fitted to the Lennard-Jones potential function. Surprisingly good agreement is found between theory and experiment. However, the value of the effective range of the potential must be increased from that which has been previously measured for intermolecular collisions to account for the presence of polarization forces in the collision.

CHAPTER I

INTRODUCTION

General

When a low energy ion collides with a diatomic molecule, either of two nonreactive processes may occur



Equation (1) represents a collision resulting only in elastic scattering of the ion. Some of the translational energy of the ion A^+ is converted into translational energy of the molecule B_2 , but the internal energy of both species is unchanged during the collision.

In Equation (2) however, not only is some of the kinetic energy of the ion converted into translational energy of the molecule, but the initial and final internal states of the molecule are no longer the same. The molecule may either lose internal energy in the collision, transferring it into translational energy of the ion, or it may gain internal energy which is observed as a discrete translational energy loss of the ion below that which would be expected for elastic scattering. This process, which is known as an inelastic collision, is the subject of this thesis.

As implied above, internal excitation of the target molecule may

be observed in the linear momentum spectrum of the scattered ions. Hence, to study the process one might direct particles of a single, known, controllable momentum onto target molecules, insuring that only single collisions occur. The momentum of the scattered particles would then be analysed to detect changes in the internal energy of the target.

These conditions are closely approximated in a beam experiment conducted at low pressures. A mass selected beam having a narrow energy distribution must be directed onto the target molecules. Molecular beams have been used to examine low kinetic energy interactions, however ions are generally chosen for the incident beam at higher energies since their kinetic energy is easily varied. Measurement of the momentum of the scattered particles is achieved in practice by determining their scattering angle, mass, and velocity.

The purpose of this work is to study the conversion of translational energy into the rotational and vibrational energy of a molecule during a collision using a beam technique. A thorough knowledge of this process is needed to explain, for example, the removal of energy from an exothermic chemical reaction or the relaxation of gases perturbed by a shock wave. In recent years a great amount of research has been conducted in this area. However, most experiments have involved the study of bulk properties of gases, while a knowledge of individual interactions is required if a theoretical model is to be tested. A beam technique is useful in providing such information.

Experimental Method

Relative differential cross sections have been obtained for the

collisional excitation of specific rotational transitions in the systems $N_2^+ + H_2$, $O_2^+ + D_2$, $Ar^+ + D_2$, and of specific vibrational transitions in the systems $N_2^+ + N_2$, $O^+ + O_2$. The variation of the relative cross sections with the velocity of the collision is studied in several of the systems. For the case of vibrational excitation, this variation in cross section is compared with that calculated on the basis of a time-dependent treatment of a forced harmonic oscillator by Treanor (1).

The experimental procedure consists of passing a low energy, mass analysed ion beam through a rotatable collision chamber containing neutral target gas. The velocity distribution of the inelastically scattered ions is scanned by a 127° cylindrical electrostatic velocity selector. Ions passed by the velocity selector are then mass analysed by a quadrupole mass spectrometer and detected. The results are analysed by a kinematic technique similar to that used by Bernstein (2) and Toennies (3). Comparison of the inelastic peak intensities for specific transitions provides the relative differential cross sections.

The present results represent the first measurement of the variation of rotational cross sections with velocity and the lowest velocities at which vibrational excitation has been studied in a beam experiment.

Review of Previous Research

It is desirable to briefly review previous studies of rotational and vibrational excitation or de-excitation using ion or molecular beams. Measurements of rotational and vibrational relaxation employing spectroscopic and transport studies have been recently reviewed by Gordon,

Klemperer, and Steinfeld (4).

Recently, independent measurements of vibrational excitation have been made by Schöttler and Toennies (3) and by Dittner and Datz (5) using time of flight spectrometers.

Toennies produced a modulated beam of Li^+ ions from the surface ionization of a lithium oxide which was velocity selected by a 127° cylindrical electrostatic sector before entering a rotatable collision chamber. The velocity spectrum of the scattered ions was analysed by measuring their time of flight over the fixed distance from the scattering chamber to the detector. Differential inelastic cross sections for ions in the laboratory (LAB) energy range of 10-50 eV were obtained for the systems $\text{Li}^+ + \text{H}_2$ and $\text{K}^+ + \text{H}_2$ from the intensity of the inelastic peak corresponding to ions backscattered in the center of mass (CM) system. Integral cross sections for the processes were obtained by measuring the smallest angle at which only elastic scattering could be observed. The probability of multiquantum vibrational transitions was found to increase with the relative energy of the collision and was in fair agreement with that predicted by the exact quantum mechanical calculation of Secrest and Johnson (6) for the system of $\text{He} + \text{H}_2$.

In Datz's apparatus, a beam of K^+ was produced by the surface ionization of K-atoms and passed into a gas-filled collision chamber without being velocity selected. The velocity spectrum of the back-scattered ions at 0° was analysed by measuring the time of flight of the ions from the scattering chamber to the detector. No cross sections for vibrational excitation were reported, but for K^+ in the LAB energy range of 50-300 eV on H_2 and D_2 , the probability of multiquantum

transitions was found, in general, to increase with relative energy.

Blythe, Grosser, and Bernstein (5) have studied the collisional de-excitation of the $J = 2$ rotational state of ortho- D_2 to $J = 0$ by K-atoms using a technique of crossed thermal beams. A velocity selected beam of K was crossed with a cooled, modulated beam of ortho- D_2 and the velocity spectrum of the scattered K-atoms scanned. The two peaks corresponding to the elastically forward and backscattered K-atoms were resolved and a peak corresponding to those K which had rotationally de-excited the D_2 was found superimposed on the backscattered elastic peak. The positions of the peaks were in good agreement with those velocities calculated from a kinematic analysis of the collision. The differential cross section for the process was obtained by subtracting the elastic backscattering peak obtained for the system $K + He$ from that of $K + D_2$. This difference in area was then compared with the area of the elastic backscattering peak. By estimating the differential elastic cross section, the differential inelastic cross section was obtained. The total inelastic cross section was inferred from data obtained in ultrasonic work on the $D_2 + D_2$ system.

In earlier experiments, Toennies (6) (7) has observed rotational excitation and de-excitation of various molecules using a rotational state selected molecular beam. Molecules in a given rotational state (J, m_j) are separated from a thermal beam of polar molecules (TlF) by an electrostatic quadrupole field and passed into a gas filled collision chamber. The rotational states of those molecules scattered less than 0.5° are determined by a second quadrupole field. Inelastic cross sections for the $(2,0) \rightarrow (3,0)$ transition were found for He, Ne, Ar, Kr,

H_2 , O_2 , air, CH_4 , SF_6 , N_2O , H_2O , CF_2Cl_2 , and NH_3 as target gases. In addition, for the case of NH_3 as a target, inelastic cross sections were determined for the transitions $(1,0) \rightarrow (2,0)$, $(2,0) \rightarrow (1,0)$, $(3,0) \rightarrow (1,0)$, $(3,0) \rightarrow (2,0)$ plus that for the $(1,0) \rightarrow (2,0)$ transition in ND_3 . This series showed that the cross sections for single quantum transitions were approximately 10 times those for which $J = \pm 2$. This selection rule was interpreted in a later paper by Toennies (8) on the basis of a time-dependent perturbation calculation for a dipole-dipole potential.

CHAPTER II

APPARATUS

Introduction

The experimental apparatus consists of two mass spectrometers mounted in tandem designed to direct a mass analysed low energy primary ion beam onto a neutral target gas and scan the mass, energy, and angular distributions of any charged particles emerging from the target region (see Figure 1).

The primary ion beam is produced by electron impact in the source and accelerated. These primary ions are then mass selected by a Nier-type mass spectrometer and the ions of desired mass decelerated to a given energy by the retarding lens system before being focused onto neutral gas molecules in the collision chamber. The scattered ions are velocity selected by a 127° electrostatic sector and mass analysed by a Residual Gas Analyser (RGA) system are suspended from the rotatable collision chamber for analysis of the angular distribution of products.

The complete apparatus is aligned on an optical bench and placed as a unit in a 32 in. ID vacuum chamber. Separate gas handling systems furnish the sample gases to the source and collision chamber. A more detailed description of the construction and operation of the individual components will be given in the remainder of this chapter.

Ion Source and Optics

The primary ion beam is generated in a gas phase electron impact

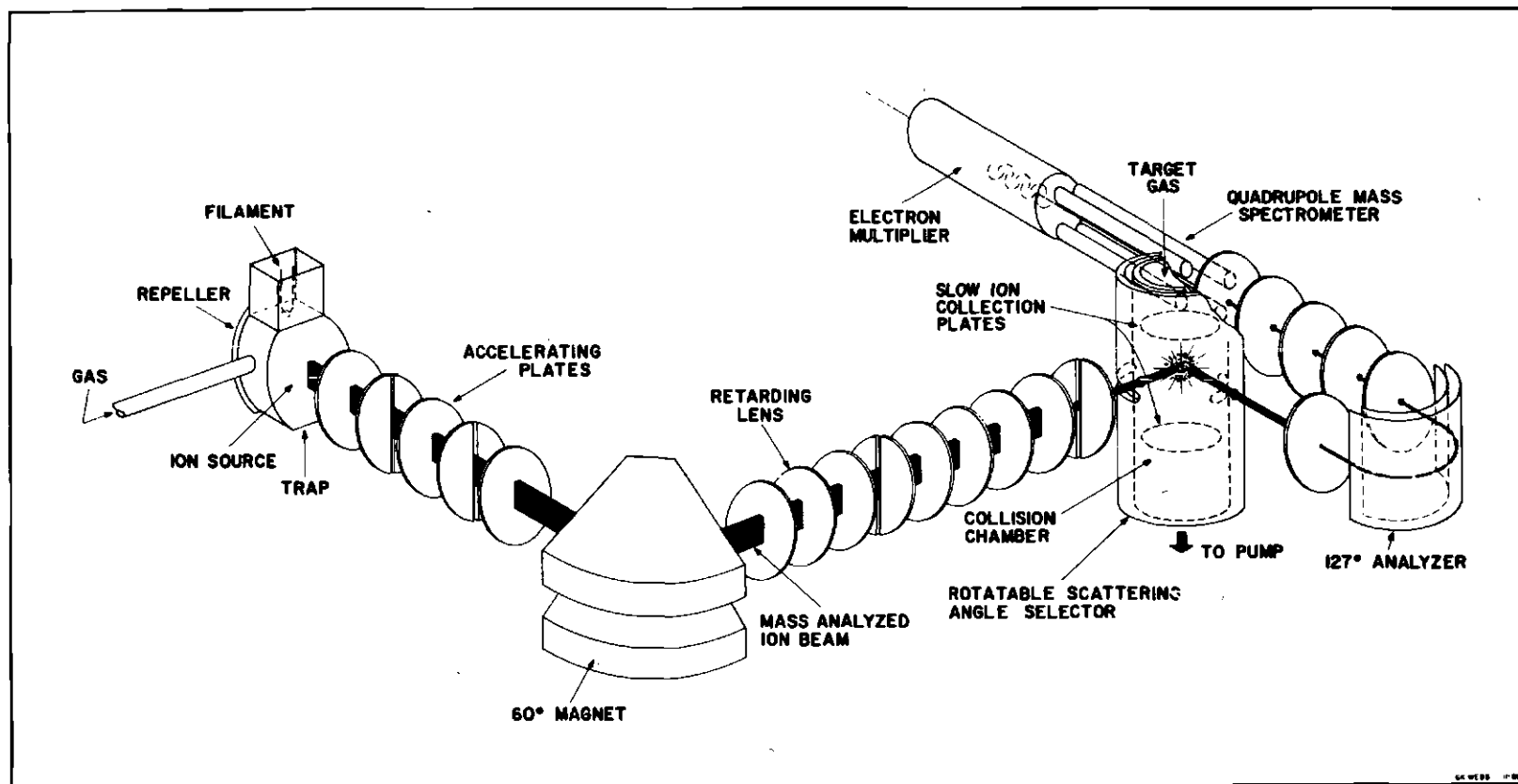


Figure 1. Functional Overall View of Experimental Apparatus.

source designed by T. F. Moran and W. M. Watson. The energy of the electrons may be varied, permitting selection of the electronic and vibrational states in which the ions are formed. The source is made of polished 304 stainless steel. Electrical insulation and lens alignment is provided by ground Pyrex glass tubing. The ion source and accelerating plates are rigidly supported from the magnet entrance slit by four stainless steel rods. Schematic diagrams of the source and accelerating plates are given in Figures 2 and 3.

The cylindrical ionization chamber is 25.40 mm in diameter and 15.86 mm in length. Electrons are accelerated from a directly heated thoriated iridium filament through a 3.18 mm diameter hole perpendicular to the axis of the ionization chamber and are collected on the opposite side by the electron trap. The filament has the dimensions 20 mm x 1 mm x 0.127 mm. It is bent into the shape of a "V" which is then suspended above the electron entrance aperture by the filament supports. During operation, the filament is covered by a stainless steel enclosure maintained at the potential of the filament. The filament is heated by a direct current of 5 to 7 amps. to give a trap current of 11 μ a. The electron beam is collimated into a small cylinder parallel to the repeller electrode by a permanent magnet outside the source having a field strength of approximately 400 gauss. To prevent reflection of electrons of unknown energy back into the ionization region, the trap is shielded by a stainless steel plate containing a 5 mm diameter hole for the passage of the electrons.

The source gas inlet is mutually perpendicular to the axis of the chamber and the electron beam. The inlet consists of a 3.00 mm ID

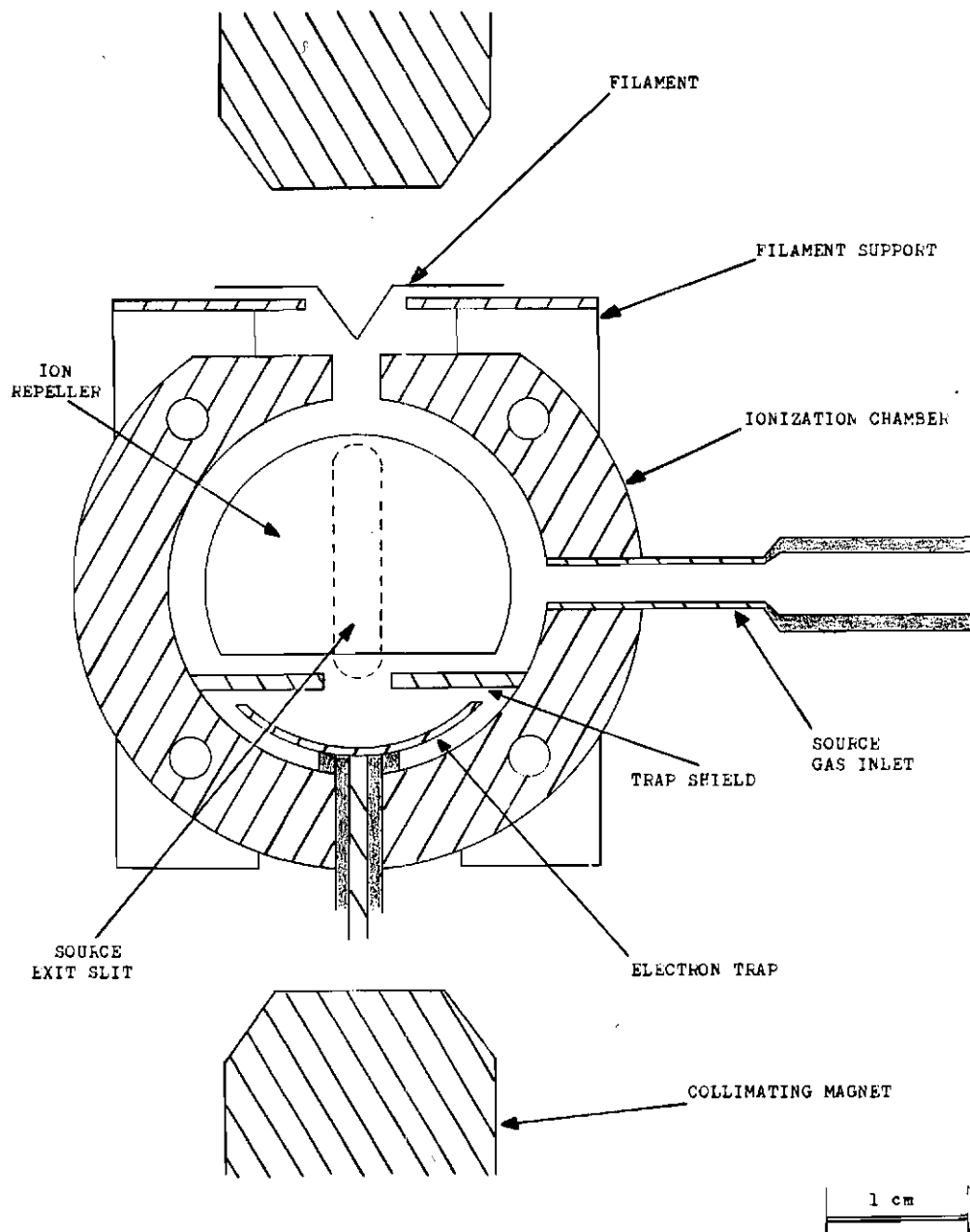


Figure 2. Schematic View of Ion Source (Front); Filament Cap Removed.

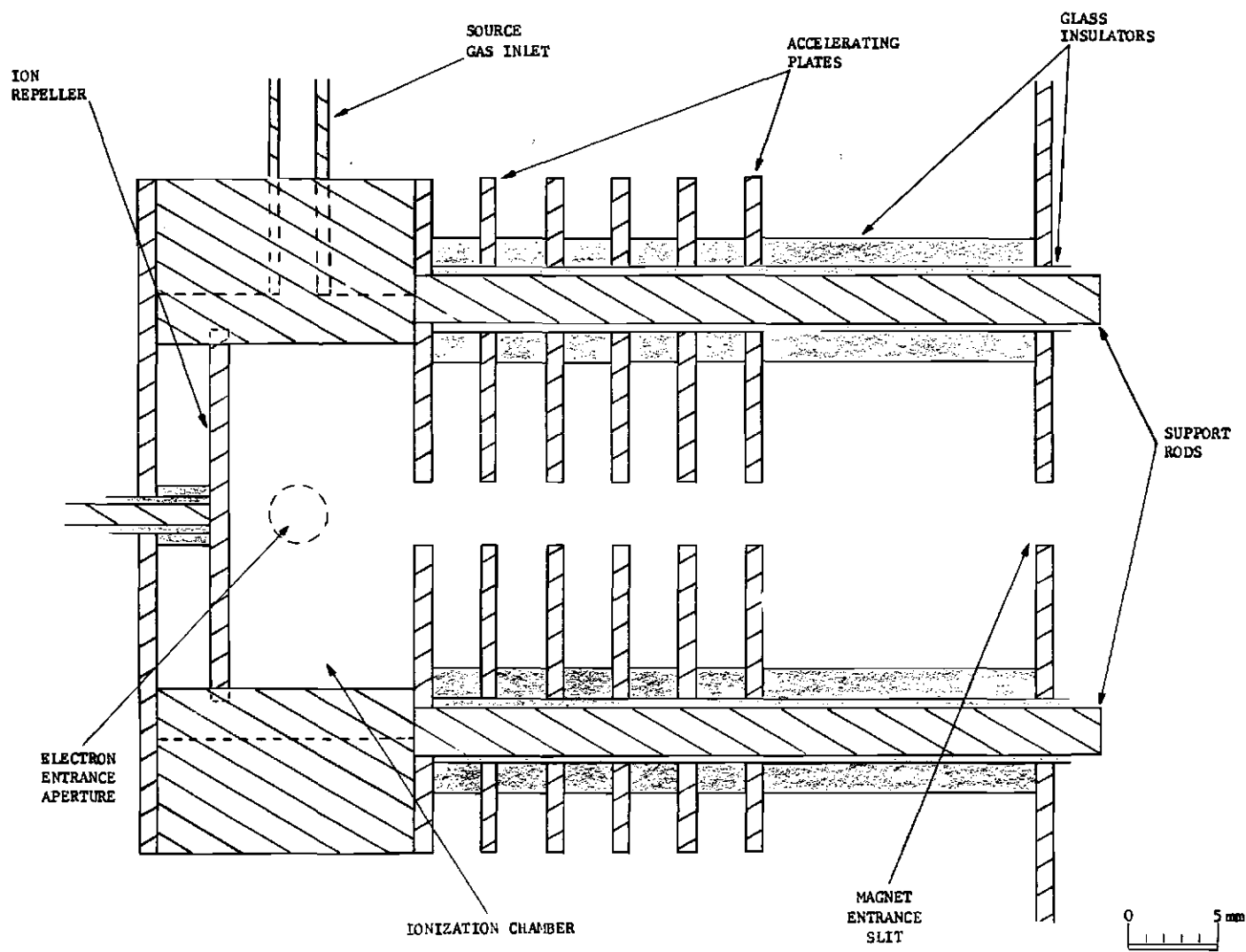


Figure 3. Schematic View of Ion Source (Top); Filament Supports Removed.

Kovar tube attached directly to the ionization chamber. Glass tubing from the gas handling system is attached to the Kovar through a graded seal. Ions formed in the center of the chamber are forced out through the 3.18×15.88 mm exit slit by a repeller electrode within the chamber.

The ion acceleration system consists of five circular plates each 0.922 mm thick and spaced by 2.74 mm. Plates 1, 3, and 5 contain slits 3.18×15.88 mm. Plates 2 and 4 are vertically split (3.97 mm wide) to allow horizontal adjustment of the ion beam to compensate for deflections of the ions due to penetration of magnetic fields from the collimating magnet and the Nier sector.

Electron emission is regulated in the Filament Power Supply to within $\pm 0.1 \mu\text{a}$. by a trap current feedback loop. The filament, trap, and repeller are floated from the ionization chamber potential by the Filament Power Supply. High voltage to the ionization chamber and the accelerating plates is supplied from a Fluke Model 408B High Voltage DC Power Supply. The relative voltages of the ionization chamber and accelerating plates are controlled through a Regulated Voltage Divider designed by G. E. O'Brian which allows independent adjustment of the ionization chamber and the two split plates. The voltage ratios between plates 1, 3, and 5 are set through fixed resistors. Typical voltages for the source to produce a 200 eV He^+ beam are given in Table 1. These potentials are essentially the same for other singly charged ions.

Table 1. Typical Potentials in the Source and Acceleration Lens System for the Production of 200 eV He⁺.
All Voltages Measured with Respect to
Instrument Ground

Source Component	Voltage
Repeller	35.67
Trap	91.75
Ionization Chamber	23.96
Filament	-36.04
Lens 1	4.28
Lens 2(R)	-30.89
Lens 2(L)	-22.45
Lens 3	-95.25
Lens 4(R)	-178.3
Lens 4(L)	-176.7
Lens 5	-200.5

Nier Mass Spectrometer

Mass selection of the primary ion beam is accomplished in a wedge-shaped 60° Nier sector (9) mass spectrometer. The magnet has a radius of 7.62 cm and, with 3.18 x 15.88 mm entrance and exit slits, a theoretical resolution defined as $\frac{M}{\Delta M}$ of 24. The pole faces, core, and yoke were machined from hot rolled steel of low carbon content. Each coil is wrapped with ten pounds of No. 24 Beldon Polythermaleze coated copper wire. Connected in series, the coils are powered by a Hyperion

Model HY-T1-330-1 Regulated Power Supply which regulates the applied voltage to within 0.02 per cent. Adjustment of mass selection is made with a Servo-Tek DC Velocity Servo (2 rpm maximum velocity, continuously adjustable to 0) attached to the 10 turn voltage control of the Hyperion. With an air gap of 35.72 mm, the magnet provides mass analysed beams of 200 eV ions up to 30 amu.

Since the primary ion beam has a high negative potential with respect to the magnet pole faces, the path of the beam through the magnet must be electrically shielded. This shielding is provided by a stainless steel enclosure which is roughly the same shape as the air gap and maintained at the potential of the beam. The side of the enclosure toward the coils is made of 90 per cent transparent nickel grid to permit removal of ions of mass higher than the selected beam which are undeflected by the magnetic field.

The magnet is attached to the optical bench via a "U" shaped aluminum stand. The acceleration and deceleration lenses are aligned by direct attachment to the magnet. The deceleration system is optically aligned with the collision chamber entrance aperture by adjusting the position of the magnet stand on the optical bench.

In practice, the resolution of this mass spectrometer has proven to be completely adequate for all purposes for which it has been used to date. It will, for instance, separate H^+ , H_2^+ , and H_3^+ to within one part in 10,000 for the 224 eV ions. Masses 36, 40, and 44 are resolved to within at least 100 ppm for the 122 eV ions.

Retarding Lens System

The mass selected ion beam is decelerated to low kinetic energies by the retarding lens system. The system used is similar to the "slot" (thick lens) system designed by Kuyatt and Simpson which has been previously incorporated into a mass spectrometer by Futrell and Miller (10). A slot lens system was chosen since it has been found (10) to have significantly greater transmission than the usual thin lens systems. Seven of the deceleration lenses were made of 3.36 mm polished 304 stainless steel with a slit geometry of 4.76 x 15.88 mm. The remaining two are 0.922 mm vertically split lenses. The lenses are rigidly attached to the magnet exit slit by four stainless steel rods. Alignment and spacing between the lenses is provided by thick-wall Pyrex glass tubing ground to within ± 0.05 mm. Relative spacing of the lenses is shown in the schematic diagram of the retarding lens system in Figure 4.

This retarding lens system provides useful He^+ beams having a LAB kinetic energy of less than 5 eV with an energy spread of 0.75 eV measured full width at half-maximum (FWHM) for 7 eV ions. It is powered by the same voltage divider used for the source. The voltage ratios between six of the lenses are set through fixed resistors. The ratios for the second retarding lens and the two split lenses are independently variable, as is the overall potential drop for the system. Table 2 lists the typical voltages applied to the retarding lens system for focusing mass selected ions having a potential of -200.5 volts onto the collision chamber whose potential is 18.83 volts.

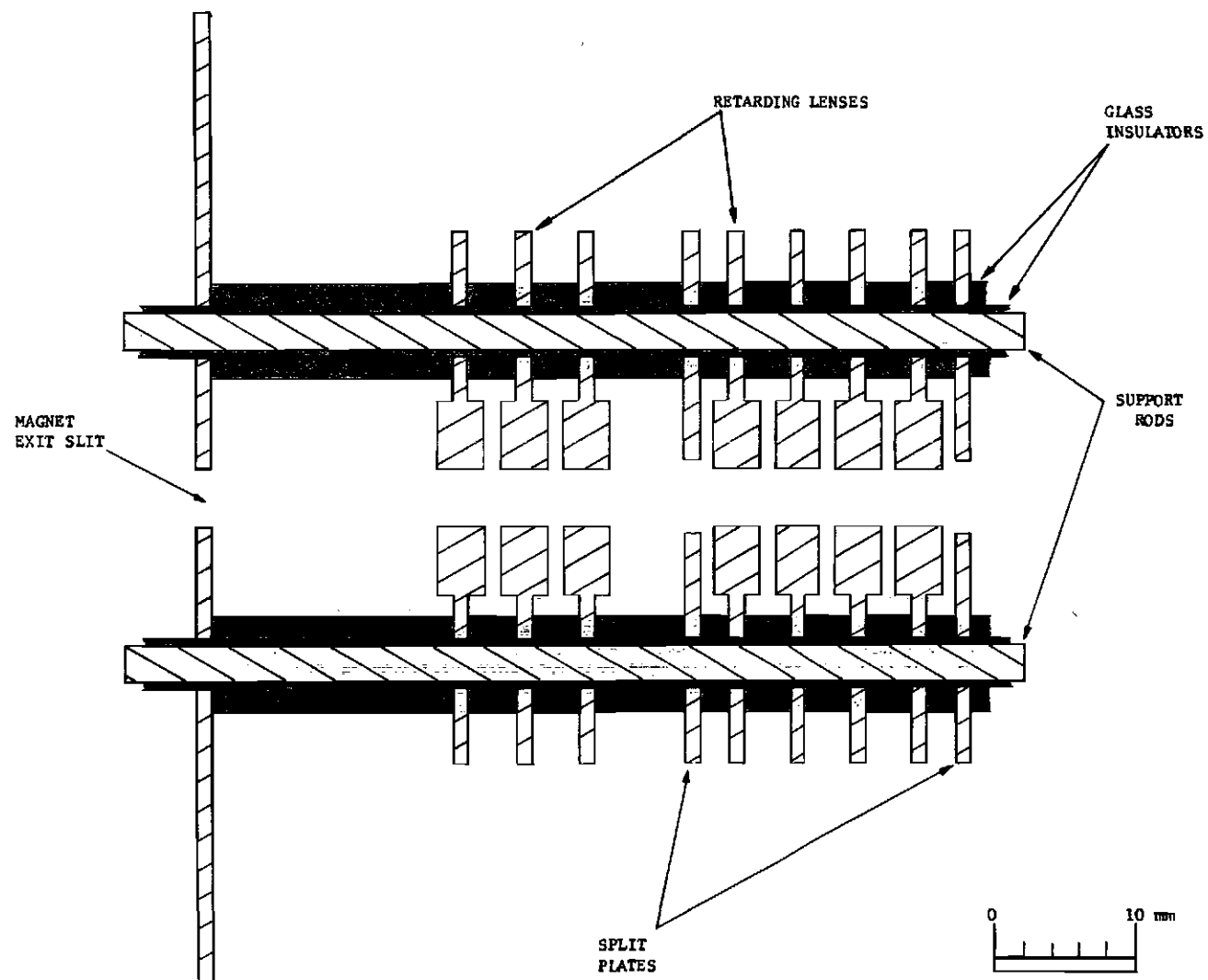


Figure 4. Schematic View of Retarding Lens System (Top).

Table 2. Typical Voltages on the Retarding Lens System to Focus 10.4 eV He⁺ into the Collision Chamber. All Voltages Measured with Respect to Instrument Ground

Lens	Voltage
1	-200.5
2	-177.3
3	-133.7
4(R)	-114.8
4(L)	-111.0
5	-79.20
6	-54.20
7	-26.81
8	1.21
9(R)	12.78
9(L)	15.00

Collision Chamber

The collision chamber was designed and built by F. C. Petty of 304 stainless steel and Teflon. The chamber is basically two concentric stainless steel cylinders with the inner cylinder attached to the optical bench. The outer cylinder is capable of rotating on two Teflon disks. Each cylinder contains one 6.35 mm diameter circular aperture and one 6.35 mm wide horizontal slit. When the outer cylinder is rotated, the outer hole moves along the inner slit. This arrangement provides a constant beam path length of 41.14 mm, poor conductance of the target gas

into the vacuum chamber, reduced reflection of the primary beam when observing secondary ions at large scattering angles, and an angular scanning range of $\pm 45^\circ$ in the LAB system. Two circular electrodes are provided at the top and bottom of the inner cylinder to permit collection of slow secondary ions. The target gas enters the collision chamber via a 3.18 mm ID stainless steel tube through the bottom of the inner cylinder.

The angular orientation of the outer cylinder is controlled through a 3600:1 gear reduction system designed and built by A. F. Hedrick. The gear system is attached to the exterior of the vacuum chamber lid. Rotation in the gear system is transferred to the outer cylinder through an Ultek Direct-Drive Rotary Motion Feedthrough. The gear system may be driven either manually or by a Type 117 constant velocity motor manufactured by the Giannini Control Corporation. Digital readout of the angular settings is provided by a turn counter attached to the gear system which may be read directly to 0.01° . The overall accuracy of the angular measurement is limited by our ability to determine 0° , which we define to be the position of the maximum intensity of the primary ion beam with no gas in the collision chamber, and by the horizontal angle subtended by the detection system (0.868°). The absolute accuracy of the angular measurement is estimated to be within $\pm 0.5^\circ$ in the LAB system.

The potential of the collision chamber is obtained from the same voltage divider used by the source and may be adjusted independently of the source and retarding lens potentials. The potential of the chamber controls the kinetic energy of the ions incident on the target gas.

Voltage differences between the ionization chamber and the collision chamber determine the kinetic energy of the primary ion beam. Normal variations in this potential of ± 0.2 per cent per hour are negligible, since they cannot be resolved by the sector during the time required for measurements.

127° Electrostatic Sector

A 127° cylindrical electrostatic sector provides energy analysis of either the primary or secondary ion beams, regardless of the masses of the ions. Since the performance of the sector is most critical for the results obtained in this paper, it will be discussed in somewhat greater detail.

Construction

The sector assembly consists essentially of four parts (see Figure 5). The outer sector is made from 1.27 mm 304 stainless steel and is connected directly to the outer collision chamber and to the quadrupole by two 6.35 mm diameter stainless steel rods. The inner sector support, which is essentially identical to the outer, is attached to the outer support by eight bolts. This inner support contains the entrance and exit apertures for the sector, which are 1.016 and 1.320 mm respectively. The entrance slit determines the scattering angle subtended by the detection system.

To the inner support are attached the inner and outer sector plates through precision ground Pyrex glass spacers. The inner plate is made of solid aluminum having an outside radius of 25.35 mm. The outer plate is an aluminum frame having an inside radius of 31.22 mm

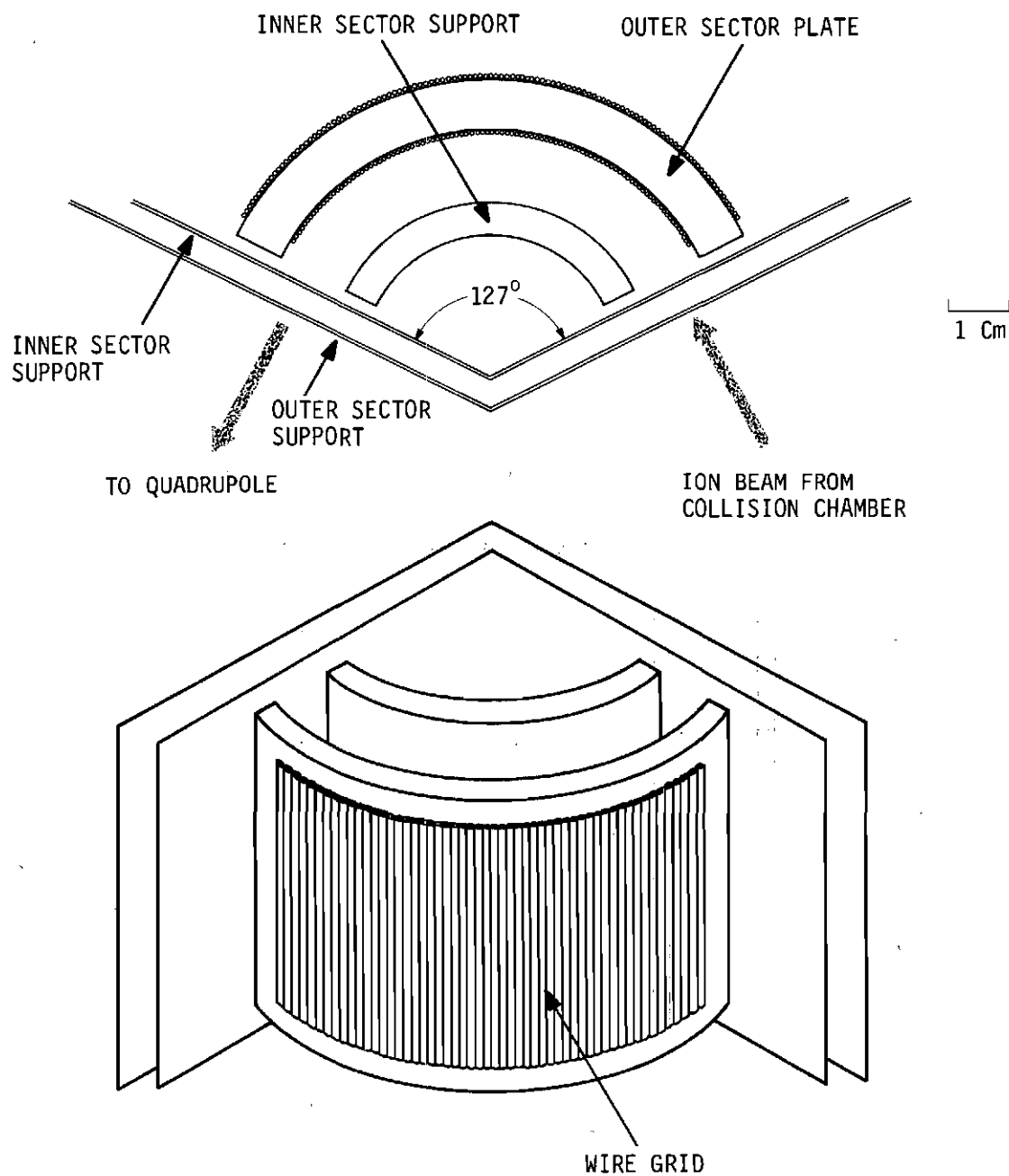


Figure 5. 127° Electrostatic Velocity Selector.

which is tightly wrapped with 0.235 mm diameter Wilstabrite stainless steel wire to approximately 20 per cent transparency. This gives the outer plate the advantage of light weight with a non-sputtering surface in addition to reducing space charge within the sector. The two aperture diameters together with the mean ion radius of 28.30 mm give the sector a theoretical energy resolution defined as $\frac{U}{\Delta U}$ of 93 (11), where ΔU is the kinetic energy spread of the focused ions measured FWHM.

Operation

The inner and outer sector supports are maintained at the potential of the collision chamber. The potentials of the inner and outer sector plates are obtained from a 45 volt battery floated at the potential of the collision chamber. Ten-turn potentiometers allow adjustment of each plate from the potential of the collision chamber as well as adjustment of the voltage difference between the plates (ΔV_{sector}). This ΔV_{sector} , which will be shown to be linear with respect to the kinetic energy of the focused ions, is stable to within ± 1 mv/hr. All voltages in the sector were measured with a Hewlett Packard Model 3440A Digital Voltmeter equipped with a Model 3445A AC/DC Range Unit to an accuracy of ± 1 mv.

Theory

The orbit of a charged particle in the radial field of two cylindrical electrostatic plates was first calculated in 1929 by Hughes and Rojansky (12). They found that at an angle of $127^\circ 17'$ both the refocusing of a diverging beam and the energy resolution of the sector were greatest.

Consider the conditions required for a particle of unit charge (e),

mass (m), and velocity (v) to describe a circular path through the sector.* The force of the field must exactly equal the centrifugal force on the particle

$$\frac{mv^2}{r_0} = \frac{-A}{r_0} \quad (3)$$

where r_0 is the mean radius of the sector and A is a constant of the field. To evaluate A in terms of measurable conditions within the sector, let

$$\Delta V_{\text{sector}} = V_{r_2} - V_{r_1} = \frac{W_{r_2-r_1}}{e} = \frac{1}{e} \int_{r_1}^{r_2} \underline{F} \cdot d\underline{l} = \frac{1}{e} \int_{r_1}^{r_2} \left(\frac{-A}{r} \right) dr \quad (4)$$

where $W_{r_2-r_1}$ is the work required to move a unit charge from the inner plate (r_1) to the outer plate (r_2), or

$$A = \frac{-e\Delta V_{\text{sector}}}{\ln(r_2/r_1)} \quad (5)$$

Substituting this value of A into equation (4), one obtains

$$\frac{mv^2}{r_0} = \frac{e\Delta V_{\text{sector}}}{r_0 \ln(r_2/r_1)} \quad (6)$$

But mv^2 is twice the kinetic energy of the particle and may be expressed as $2eU$, where U is the energy of the particle in electron volts. Equation (6) now becomes

*This derivation is essentially that of Hughes and McMillen (13).

$$\Delta V_{\text{sector}} = 2U \ln \left(\frac{r_2}{r_1} \right). \quad (7)$$

Hence ΔV_{sector} should vary linearly with respect to the kinetic energy of the ions focused. It should be noted that ΔV_{sector} for a given sector depends only on the energy of the ions focused, not on the mass or charge of the ions as in the case of magnetic selection.

Hughes and McMillan (13) calculated the potential difference required to focus electrons of a given energy in their selector and found it to be 0.9 per cent higher than their experimentally observed value. In like manner, for the variation of ΔV_{sector} with electron energy, their theoretical and experimental ratios agreed to within 0.7 per cent over a range of electron energies from 50 to 200 eV.

Calibration

The sector is operated with the potentials of the inner and outer plates symmetric about the potential of the collision chamber. The ratio between ΔV_{sector} and the ion kinetic energy was determined using a He^+ beam by varying only the collision chamber potential and then readjusting ΔV_{sector} to regain maximum beam intensity. ΔV_{sector} was found to vary linearly with He^+ kinetic energy between 5 and 21 eV within ± 0.05 eV. A change in ΔV_{sector} of 1.000 volts implied a change in ion kinetic energy of 2.50 eV. Exactly the same ratio was calculated for this sector using equation (7).

Absolute calibration of the energy scale of the sector required determining the potential difference through which the He^+ were accelerated from the point at which they were formed until they entered the

sector. This potential difference is the sum of the voltage between the ionization chamber and the collision chamber and the effective potential which repelled the ions from the ionization chamber. Due to the positive potential applied to the repeller electrode and the penetration of fields from the filament, trap, and accelerating plates, the ionization chamber is not an equipotential volume, but, rather, it contains the sum of several potential gradients. Resistance plotting of the equipotentials within the ionization chamber indicates they are parallel to the face of the repeller electrode in the region in which the ions are formed. The ions are formed in a collimated cylindrical volume parallel to the repeller electrode, hence the potential difference through which these ions are accelerated out of the ionization chamber will be the same as that through which the electron beam is accelerated within the ionization chamber.

To measure this potential difference, He^+ current was plotted versus the applied voltage between the filament and the ionization chamber. By extrapolating the linear portion of this plot to zero ion current, an apparent ionization potential for He of 23.79 ± 0.10 eV was obtained. Comparison of this value with the accepted spectroscopic value of 24.580 eV (14) implies that the electrons and, therefore, the ions are accelerated by 0.80 ± 0.10 eV within the ionization chamber. Hence 0.80 eV has been added to the potential difference between the ionization chamber and the collision chamber measured during the relative calibration of the sector to give the true energy of the He^+ selected by the sector. The fact that the contribution is less than 10 per cent of the applied repeller voltage is reasonable since the repeller voltage

may be varied several volts without significantly changing the kinetic energy of the ion beam.

The arithmetic mean of 15 repetitive determinations of ΔV_{sector} is given in Table 3 for several representative values of He^+ kinetic energies between 10 and 20 eV. The corresponding values calculated using equation (7) are listed for comparison.

Table 3. Comparison of Calculated Values of ΔV_{sector} with Observed Values for Various Kinetic Energies of He^+

Kinetic Energy (eV)	ΔV_{sector}	
	Eqn. (7)	Observed
10.0	4.011	3.96
12.0	4.814	4.76
15.0	6.017	5.97
18.0	7.220	7.18
20.0	8.023	7.97

Residual Gas Analyser System

An Ultek-EAI QUAD 150A Residual Gas Analyser is used to mass analyse the energy selected ion beam. The analyser system consists of a 35 mm axial beam ionizer, a rf/dc quadrupole mass spectrometer, and an electron multiplier detector.

The quadrupole gives linear mass separation with a resolution of unity when resolution is defined as the separation in amu of two mass peaks of equal height when the valley between them is 10 per cent

the peak height. It should be noted that the quadrupole's mass analysis is essentially independent of ion velocity.

The entrance to the quadrupole is fitted with an Ultek-EAI 35 mm axial beam ionizer. During beam measurements, the ionizer is maintained at ground potential with the exception of the first acceleration plate which remains at -106 volts. Significant grazing of the ion beam with the wire grid normally present at the entrance to the ionizer necessitated removing the grid. The ionizer assembly is used only for verification of the quadrupole's mass scale and for detecting leaks in the vacuum system.

The mass selected ion beam is detected by an EAI 14 stage Be-Cu electron multiplier having a gain of approximately 10^5 and a response time of better than 10^{-4} seconds. The gain of the multiplier is specified by the manufacturer to be stable after an initial decrease of 0.05 per cent during the first few days of operation.

The current at the multiplier is measured with a Keithley Model 417 High-Speed Picoammeter having 18 current ranges from 10^{-13} to 3×10^{-5} amps full scale. Use of the current suppression adjustment of the instrument permits full scale display of 0.1 per cent signal variations. Zero drift is specified to be less than one per cent per eight hours. The output from the Keithley is displayed on a Leeds and Northrup Speedomax W/L two pen strip chart recorder.

The complete RGA assembly is 28 cm long and weighs approximately two pounds. It is suspended from the outer sector support by two 6.35 mm diameter 304 stainless steel rods.

Vacuum System

The entire spectrometer is enclosed in a 15 in. x 32 in. ID cylindrical vacuum chamber made of 304 stainless steel. Access to the contents of the chamber is provided through the 32 in. top flange. Four four inch Ultek "Curvac" flanges are positioned radially about the chamber. One of these serves as a viewing port to facilitate alignment of the Rotary Direct Drive coupling to the collision chamber. The second has been specially modified to permit electrical feedthrough into the chamber as well as for connecting the source ionization chamber and collision chamber with the gas sample handling system. The remaining two flanges are equipped with 15 KVA Ceramaseal High Vac electrical feedthroughs.

A one and one-half inch Curvac flange is centered on the lid of the chamber for the attachment of the rotary motion feedthrough to the collision chamber. Two one and one-half inch Curvac flanges on the floor of the chamber furnish all electrical feedthroughs required for the RGA assembly. All flanges are heliarc welded on the inside of the chamber and fitted with metal "O" rings.

Pumping is through a six inch flange centered in the floor of the vacuum chamber by a NRC Model VHS-6 six-inch oil diffusion pump equipped with a NRC Type 0317-6 Molecular Sorbent (Zeolite) and a water cooled Cold Cap. The diffusion pump has a maximum pumping speed of 2400 liters per second for air. The backing pump is a Welch Duo-Seal Model 1397.

A vacuum of 10^{-7} torr may be easily attained within four hours from atmospheric pressure without bake-out of either the chamber or its

contents. The ultimate is limited by degassing of the magnet coils. This degassing of the coils leads to an increase in chamber pressure above 10^{-7} torr only when the Nier spectrometer is operated at its highest mass range for more than four hours. Overall chamber pressure is measured with a CVC Type GPH-100A discharge vacuum gauge having three pressure ranges from 2.5×10^{-2} to 1×10^{-7} torr.

Sample Gas System

The gas samples for the primary and target beams are handled by an all glass system which provides more than 12 liters of ballast each for the source and target gases. A static pinhole leak in each inlet line insures a pressure reduction of approximately 10^3 on the chamber side. The flow rate into the source and target regions may be kept constant during a series of measurements by adjusting the pressure in the ballast. The system is pumped by a three inch mercury diffusion pump equipped with a liquid nitrogen cold cap, and by a Welch Duo-Seal Model 1400 backing pump.

CHAPTER III

KINEMATICS OF THE COLLISION

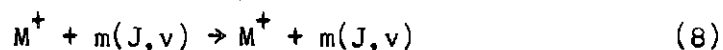
The following notation is used throughout the discussion:

E_0	LAB energy of ions in incident beam
\vec{P}_0	LAB momentum of ions in incident beam
\vec{V}_0	LAB velocity of ions in incident beam
M	mass of incident and detected ions
E, E'^*	LAB energy of scattered ions
\vec{P}, \vec{P}'	LAB momentum of scattered ions
\vec{V}, \vec{V}'	LAB velocity of scattered ions
E_e, E'_e	LAB energy of elastically scattered ion
\vec{P}_e, \vec{P}'_e	LAB momentum of elastically scattered ion
\vec{V}_e, \vec{V}'_e	LAB velocity of elastically scattered ion
E_i, E'_i	LAB energy of inelastically scattered ion
\vec{P}_i, \vec{P}'_i	LAB momentum of inelastically scattered ion
\vec{V}_i, \vec{V}'_i	LAB velocity of inelastically scattered ion
m	mass of target molecule
K	LAB energy of scattered target molecule
\vec{p}	LAB momentum of scattered target molecule
$\Delta\epsilon$	relative energy loss of incident ion (in CM system)
ΔE	LAB energy loss of incident ion

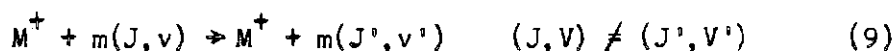
*The superscript (') is used to distinguish quantities associated with those ions backscattered in the CM system when distinction between forward and backscattering is desired.

μ	reduced mass of system
E_s	initial relative kinetic energy of collision (in CM system)
\vec{F}	LAB momentum of the center of mass
\vec{R}	LAB momentum of scattered ion with respect to CM
\vec{R}_e	LAB momentum of elastically scattered ion with respect to the CM
\vec{R}_i	LAB momentum of inelastically scattered ion with respect to the CM
θ	LAB scattering angle of ion
Φ, Φ'	CM angle of scattered ion
Φ_e, Φ'_e	CM angle of elastically scattered ion
Φ_i, Φ'_i	CM angle of inelastically scattered ion.

Consider a collimated beam of ions of mass M and energy E_0 incident on target molecules of mass m which are at rest in the laboratory (LAB) system. Some of the ions may be elastically scattered by the molecules



and some may transfer a quantum of energy $\Delta\varepsilon$ into the internal degrees of freedom of the target molecule



undergoing an inelastic collision. The purpose of this section is to explain the kinematics of the detected ion M^+ which will be observed in the LAB system after it has interacted with a target molecule in the center of mass (CM) system.

If only in-plane scattering processes are considered, the

problem* is two dimensional and may be represented as shown in Figure 6. Applying conservation of energy to the collision

$$E_o = E + K + \Delta E \quad (10)$$

where $\Delta E = 0$ for elastic processes and $\Delta E > 0$ for inelastic excitation.

In terms of the momentum components of the particles

$$\frac{p_o^2}{2M} = \frac{p_x^2 + p_y^2}{2m} + \frac{p_x^2 + p_y^2}{2M} + \Delta E \quad (11)$$

Since only ions of mass M will be observed by the detector, only the equations of motion of the ion will be considered here. The results, however, are of essentially the same form for either the molecule or the ion.

p_x and p_y may be eliminated from Equation (10) by employing conservation of the linear momentum of the two particles along the X and Y axes

$$P_o = P_x + p_x \quad (12)$$

$$0 = P_y + p_y$$

to obtain

$$\frac{p_o^2}{2} \left(\frac{m - M}{mM} \right) = \frac{p_x^2}{2M} + \frac{p_y^2}{2M} - \frac{P_o p_x}{m} + \Delta E. \quad (13)$$

*The formulation of this problem is based on the procedure used by Henglein, Lacmann, and Jacobs (15) who applied it to bimolecular reactions. Similar conclusions have been reached by Blythe, Grosser, and Bernstein (2) who have applied it to rotational de-excitation using crossed beams and Schöttler and Toennies (3) for the case of vibrational excitation using a time-of-flight technique.

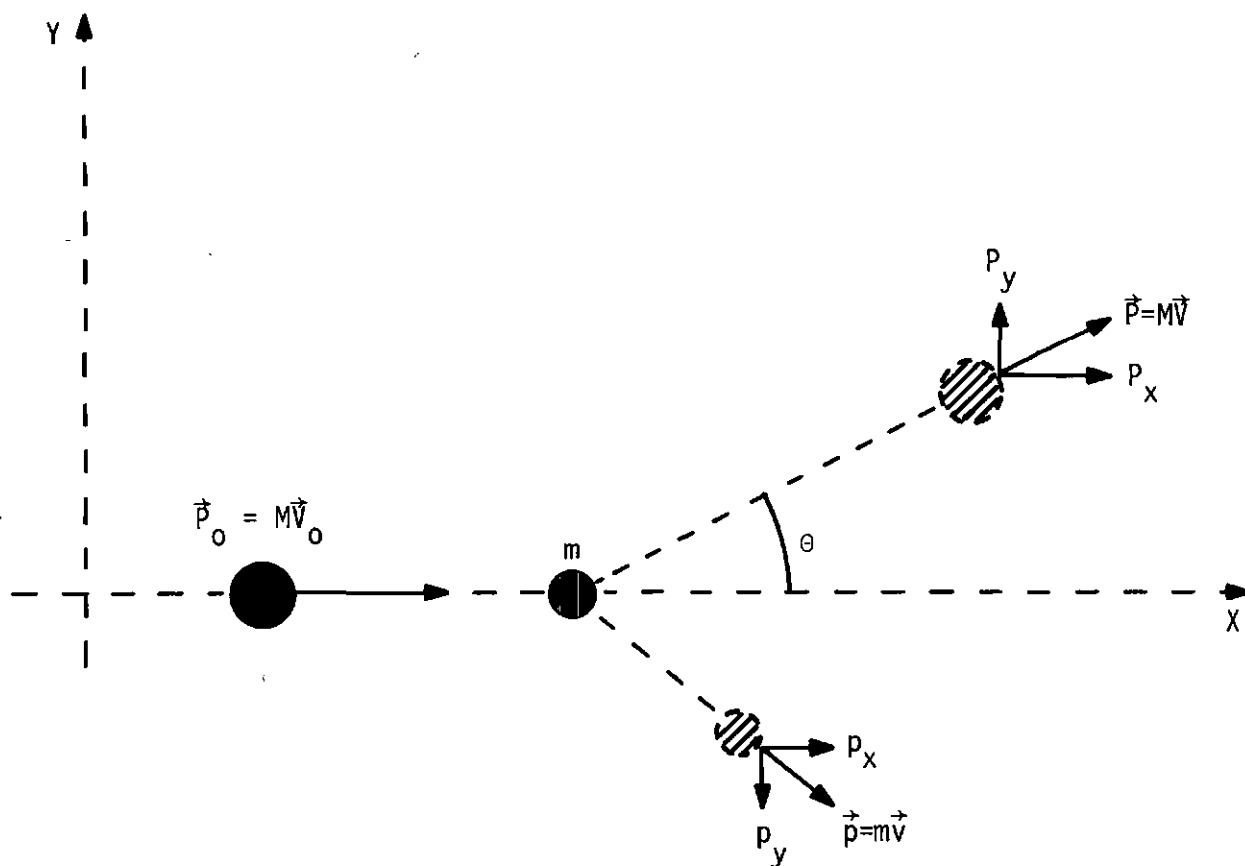


Figure 6. Schematic Representation of Collision in LAB System.

Multiplying both sides of Equation (13) by 2μ and completing the square on the terms containing P_x , one obtains

$$(P_x - \frac{M}{M+m} P_o)^2 + P_y^2 = P_o^2 \left[\left(\frac{M}{M+m} \right)^2 - \frac{M}{M+m} \right] + 2\mu \left(\frac{P_o^2}{2M} - \Delta E \right) \quad (14)$$

where the term $\frac{M}{M+m} P_o$ is the momentum of the center of mass, F .

The right hand side of Equation (14) may be rearranged to obtain

$$(P_x - F)^2 + P_y^2 = R^2 \quad (15)$$

where

$$R = 2\mu(E_s - \Delta E)^{1/2} \quad (16)$$

is the momentum of the scattered ion relative to the center of mass,

$$E_s = 1/2 \mu V_o^2 \quad (17)$$

is the relative kinetic energy of the collision, and

$$\Delta E = \frac{(M+m)}{m} \Delta \epsilon \quad (18)$$

is the inelastic energy loss of the incident ion in the LAB system.

Equation (15) may be represented as a circle of radius R in momentum space (P_x, P_y) whose origin is displaced along the P_x axis a distance of F (see Figure 7). If an ion detector is placed at an angle θ to the path of the incident beam in the plane of scattering and the velocity spectrum of the scattered ions is scanned, two peaks will be

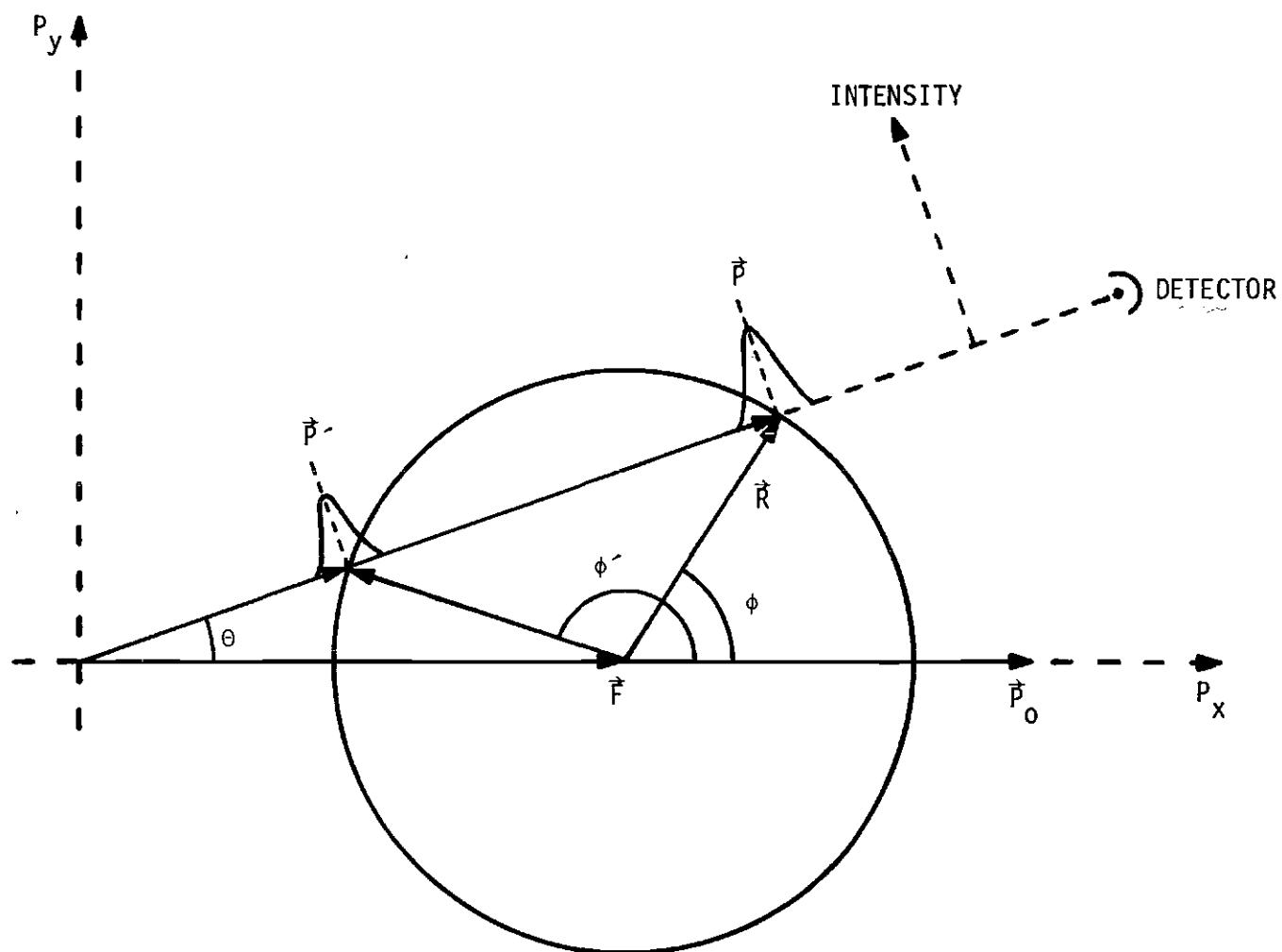


Figure 7. Schematic Momentum Vector Diagram for Arbitrary Collision Showing Initial and Final Coordinates of Scattered Ion in LAB and CM Systems.

observed having momenta \vec{P} and \vec{P}' , corresponding to those ions which have been scattered through angles Φ and Φ' in the CM system.

If both elastic and inelastic processes can occur in the collision, the momentum space of the ion will contain two concentric circles of radii R_e and R_i drawn from the vector \vec{F} (see Figure 8). The velocity spectrum of the ions observed at the detector will now yield four peaks, corresponding to scattering in the CM system at angles Φ_e , Φ_i , Φ'_e , and Φ'_i . Considering only the forward scattered peaks (unprimed), the observed energy of the elastically scattered ions may be calculated as a function of Φ_e from the magnitude of the vector P_e

$$\begin{aligned} |\vec{P}_e|^2 &= (|\vec{F}| + |\vec{R}_e| \cos \Phi_e)^2 + (|\vec{R}_e| \sin \Phi_e)^2 \\ &= F^2 + 2FR_e \cos \Phi_e + R_e^2. \end{aligned} \quad (19)$$

Upon substitution of the definitions of F and R_e , Equation (19) may be expressed in terms of the LAB energy of the elastically scattered ion

$$E_e = \frac{P_e^2}{2M} = \left[\frac{M^2 + 2Mm \cos \Phi_e + m^2}{(M + m)^2} \right] E_o. \quad (20)$$

In a like manner, the observed energy of the forward scattered inelastic peak may be obtained

$$\begin{aligned} |\vec{P}_i|^2 &= (|\vec{F}| + |\vec{R}_i| \cos \Phi_i)^2 + (|\vec{R}_i| \sin \Phi_i)^2 \\ &= F^2 + 2FR_i \cos \Phi_i + R_i^2, \end{aligned} \quad (21)$$

or

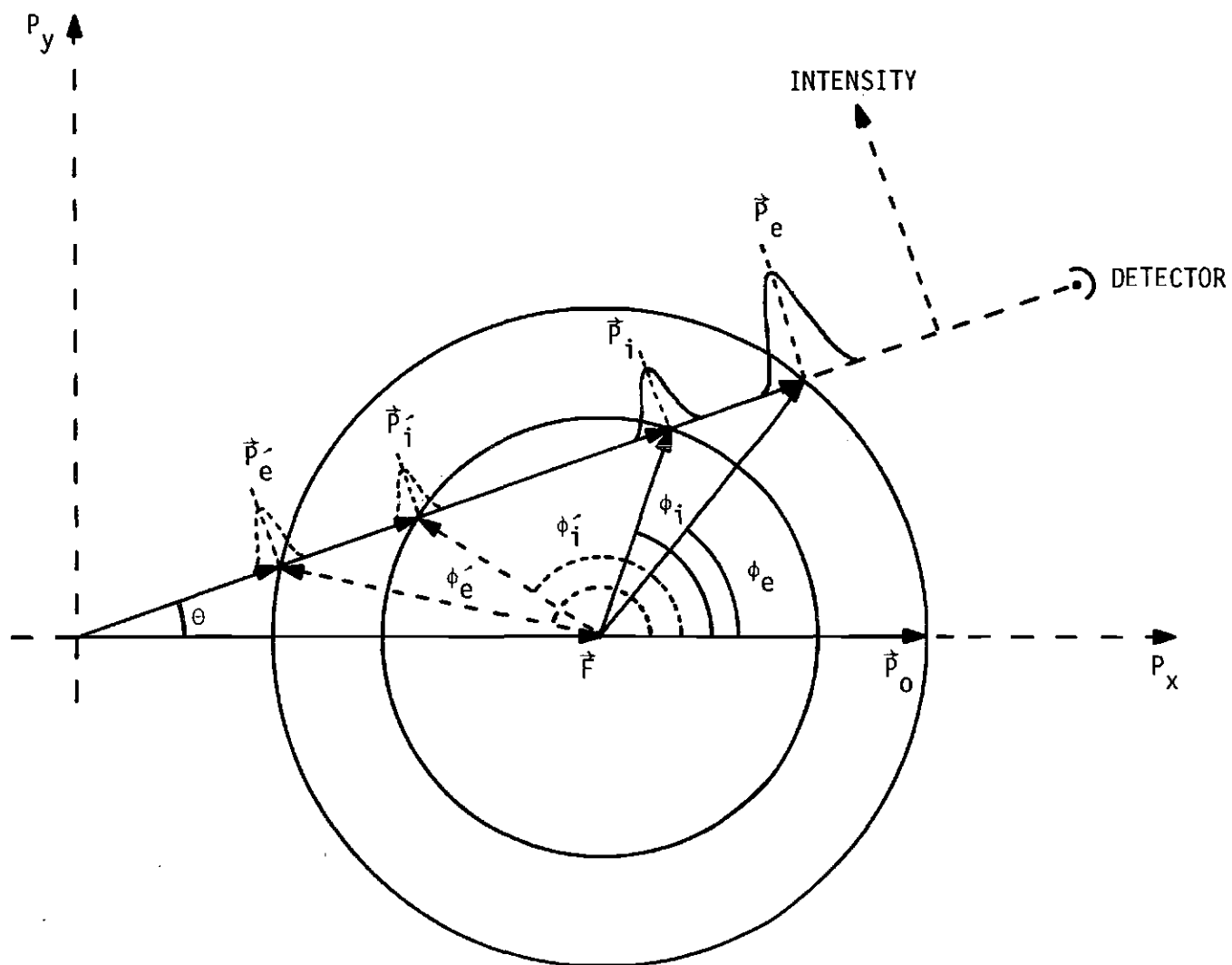


Figure 8. Schematic Momentum Vector Diagram for both Elastic and Inelastic Collisions Showing Initial and Final Coordinates of Scattered Ion in LAB and CM Systems.

$$E_i = \frac{M^2 + m^2}{(M + m)^2} E_o + \frac{2MmE_o}{(M + m)^2} \left[\left(1 - \frac{\Delta E}{E_s} \right)^{1/2} \cos \Phi_i - \frac{m\Delta E}{M + m} \right]. \quad (22)$$

If $\frac{\Delta E}{E_s}$ is small, the square root may be expanded in a binomial series in which only the first two terms are retained* to obtain Equation (22) in the more useful form

$$E_i = \left[\frac{M^2 + 2Mm \cos \Phi_i + m^2}{(M + m)^2} \right] E_o - \frac{\Delta E}{M + m} (m + M \cos \Phi_i). \quad (23)$$

Subtracting Equation (23) from Equation (20) one obtains the observed shift in the inelastic peak from the elastic peak

$$E_e - E_i = \frac{2MmE_o}{(M + m)^2} (\cos \Phi_e - \cos \Phi_i) + \frac{\Delta E}{M + m} (m + M \cos \Phi_i) \quad (24)$$

where Φ_e may be calculated from (16)(17)

$$\tan \theta = \frac{\sin \Phi_e}{M/m + \cos \Phi_e} \quad (25)$$

and Φ_i from**

$$\cos \Phi_i = 1 - \left[\frac{(M + m)^2 E_i \sin^2 \theta}{m^2 E_o \left(1 - \frac{\Delta E}{E_s} \right)} \right]^{1/2}. \quad (26)$$

* A four per cent error for $\frac{\Delta E}{E_s} = 0.5$.

** See Figure 8.

In many cases it is quite accurate to assume $\cos \Phi_i = \cos \Phi_e$, whereupon Equation (26) reduces to

$$E_e - E_i = \frac{\Delta E}{M + m} (m + M \cos \Phi_e) . \quad (27)$$

As an example, consider the case of a beam of 12.20 eV $(\text{Ar}^{40})^+$ incident on D_2 . The detector monitors the velocity spectrum of only $(\text{Ar}^{40})^+$ and may be placed at any angle θ with respect to the incident beam. For the $J = 0 \rightarrow J = 2$ rotational transition of $X \sum_g^+ D_2$, $B_e = 30.429 \text{ cm}^{-1}$ (18), hence $\Delta e = 0.02263 \text{ eV}$ and $\Delta E = 0.2489 \text{ eV}$. The CM elastic scattering angle Φ_e corresponding to the LAB angle θ may be calculated from Equation (25) and substituted into Equations (20) and (27) to obtain an approximate value of E_i . This E_i is then used in Equation (26) to obtain an approximate value of Φ_i which, in turn, is substituted into Equation (24) to obtain the shift in the inelastic peak from the elastic peak. While in most cases the accuracy of the results thus obtained is more than adequate for the purpose of this paper, higher accuracy may be achieved by an iterative procedure. The results of this calculation for three values of θ are given in Table 4.

Table 4. Calculated Observables for the Excitation of the $J = 0 \rightarrow J = 2$ Rotational Transition of $X^1\Sigma_g^+ D_2$ by 12.20 eV (LAB) $(Ar^{40})^+$ at Different Laboratory Angles of Detection

θ (deg.)	Φ_e (deg.) Eqn. 25	Φ_i (deg.) Eqn. 26	E_e (eV) Eqn. 20	$E_e - E_i$ (eV) Eqn. 27	$E_e - E_i$ (eV) Eqn. 24
3	34.55	36.03	11.84	0.209	0.216
1	11.07	11.47	12.16	0.245	0.244
0	0	0	12.20	0.249	0.249

CHAPTER IV

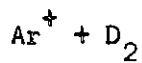
EXPERIMENTAL PROCEDURES AND RESULTS

General

The experimental apparatus and general operating conditions used in this work have been presented in Chapter II. Several additional conditions particular to the results presented in this chapter are listed below.

The ions in the primary beam were resolved from their more abundant isotropic impurities to within 0.1 per cent. The sources and purities of the target gases were as follows: D_2 , Matheson C. P. Grade (99.5 atom per cent); H_2 , Matheson Prepurified Grade (99.95 per cent min.); O_2 , Matheson E. D. Grade (99.7 per cent min.). All velocity scans were obtained by varying ΔV_{sector} at a rate of 2 mv/sec or less. The detector position was maintained at zero degrees in the LAB system and subtended a half-angle of 22.1 minutes in the horizontal plane. The observed ions of the incident beam were completely resolved from those masses corresponding to possible charge transfer or reactive collision products.

Rotational Excitation



The observed velocity spectrum of the forward scattered Ar^+ consists of ions from the primary beam which have not undergone a collision, elastically scattered ions and ions which have been inelastically scattered. The velocity distribution of the incident beam

varied from 0.9 eV FWHM for the 16 eV ions to 1.2 eV FWHM for the 10 eV ions. This inherent width of the primary ion beam and its broadening due to elastic scattering within the collision chamber prevented the complete separation of the inelastic scattering peaks from the primary Ar^+ beam. Rather, the inelastic peaks appear as quite distinct humps superimposed on the spectrum of the primary beam. Figure 9 shows the velocity spectrum resulting from 12.90 eV Ar^+ on D_2 .

To determine the intensities of the inelastic peaks, control spectra were obtained for the system $\text{Ar}^+ + \text{He}$ in which only elastic scattering is possible. These velocity spectra were unstructured and had the same general shape as those of $\text{Ar}^+ + \text{D}_2$. Identical intensities, however, could be obtained only in the region of the tails of the peaks. This is not surprising, since the effective sizes and elastic scattering potentials of the two targets could not be expected to be the same, although their masses are essentially identical. Hence, the intensity of the spectra obtained for $\text{Ar}^+ + \text{He}$ had to be extrapolated to those for $\text{Ar}^+ + \text{D}_2$. The dashed line in Figure 9 represents the result of this extrapolation.

Direct subtraction of the two curves results in the rotational spectrum of D_2 shown in Figure 10. Also shown are the positions of the peaks predicted by Equation (24), where $\Delta\epsilon$ is the energy difference between the rotational levels of a diatomic molecule

$$\Delta\epsilon_{m,n} = [J_n(J_n + 1) - J_m(J_m + 1)]B_e. \quad (28)$$

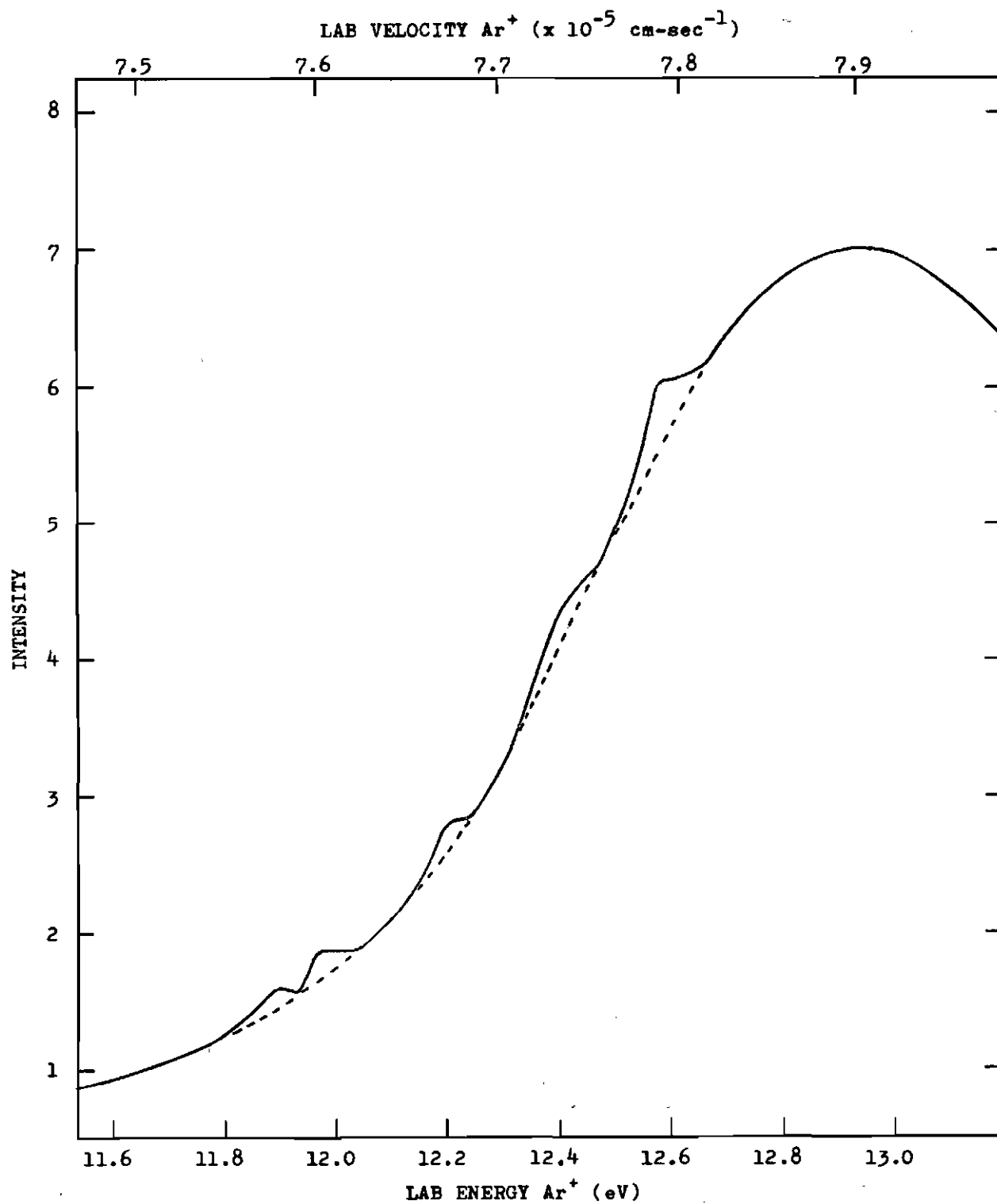


Figure 9. Velocity Spectrum of 12.90 eV LAB Ar^+ in System $\text{Ar}^+ + \text{D}_2$.

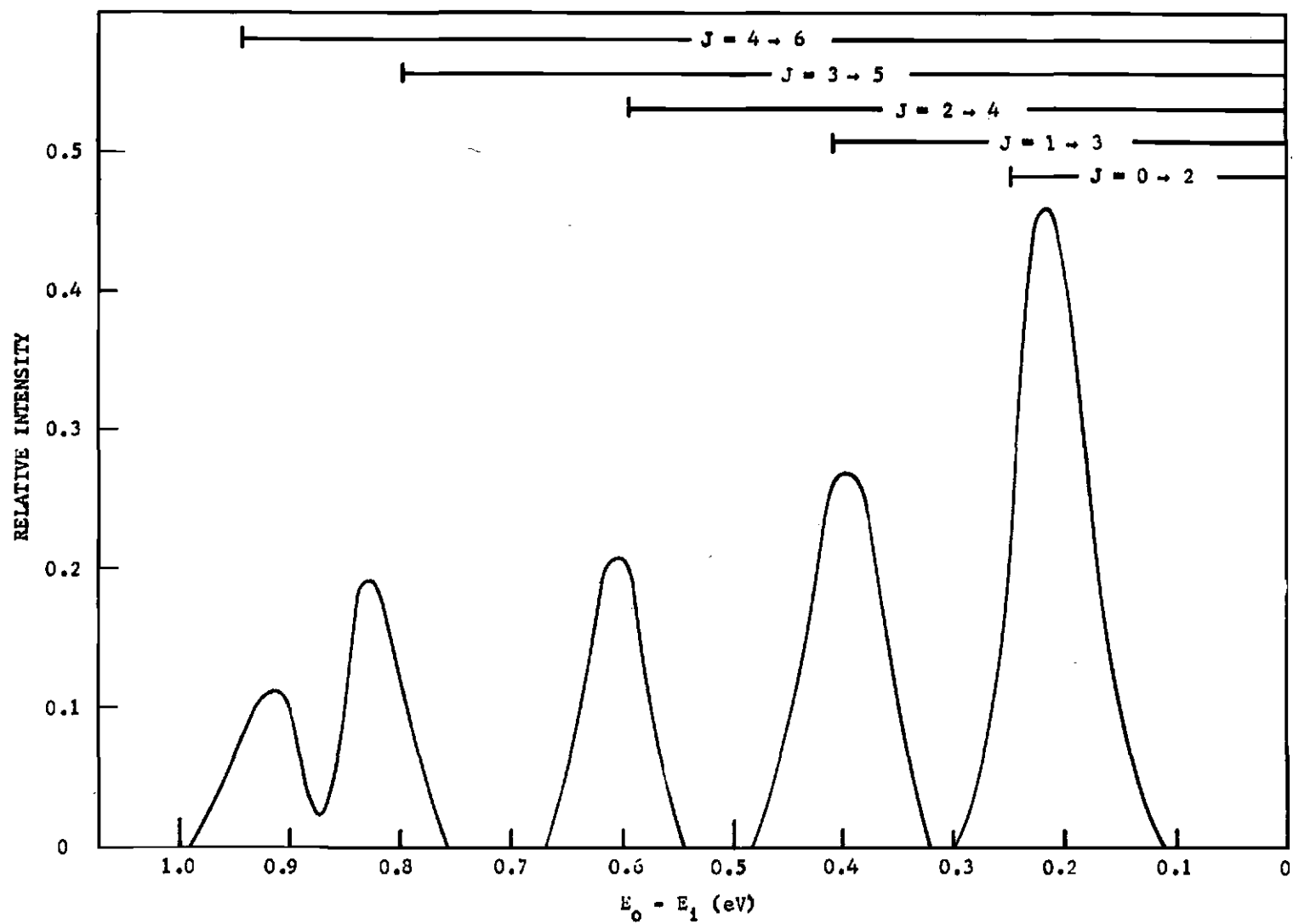


Figure 10. Rotational Spectrum of D_2 Resulting from Collisional Excitation by 12.90 eV LAB Ar^+ .

An extensive list of values for the rotational constants (B_e) of most diatomic molecules is given in Reference (18). For the particular case of D_2 , $B_e = 0.0037714$ eV. The maximum difference between predicted and measured energies of the inelastic peaks for all spectra in this system was five per cent.

It should be noted that only transitions corresponding to $\Delta J = +2$ are observed. This is readily explained by a consideration of the symmetry requirements for the wave function of the target molecule. Since a deuteron is a boson, the total wave function for D_2 must be symmetric with respect to the interchange of the coordinates of the two nuclei. If the molecule's electronic, vibrational, rotational, and nuclear coordinates are separable, the total wave function may be written as the product of electronic, vibrational, rotational, and nuclear wave functions.

The electronic and vibrational wave functions depend only on distance and are, therefore, symmetric with respect to interchange of the two nuclei. Thus the symmetry of the total wave function must depend only on the symmetries of the rotational and nuclear wavefunctions.

The spin states in D_2 with total nuclear spins of 0 and 2 are symmetric having a six-fold degeneracy. Those states in which the total spin is 1 are antisymmetric and have a degeneracy of 3. The molecules in which the nuclear spin states are even are called ortho- D_2 , while those in which they are odd are called para- D_2 . It is easily shown (19) that the ratio of the number of molecules of ortho- D_2 to that of para- D_2 in deuterium in equilibrium at room temperature is equal to the ratio of

the degeneracies of their respective spin states. In this case, the ratio is two.

The wave function for rotational states in which J is even is symmetric, while for states of odd J the wave function is anti-symmetric, with respect to the interchange of the nuclei. Hence, for the total wave function to be symmetric, only rotational states for which J is even can occur in ortho- D_2 . Only those for which J is odd occur in para- D_2 .

Of course transitions for which ΔJ is an integral multiple of ± 2 are permitted by the above consideration, but such transitions have not been observed in the spectra of this system. Considering these transitions may be hidden in detector noise, an upper limit to the probabilities for the transitions $J = 0 \rightarrow 4$ and $J = 1 \rightarrow 5$ may be set at three per cent those for $J = 0 \rightarrow 2$ and $J = 1 \rightarrow 3$ respectively.

To obtain relative transition probabilities from the relative intensities of the inelastic peaks, the intensities must be weighted to take into account differences in the relative populations of the rotational ground states of the target. The Boltzmann distribution calculated for D_2 at 300°K is given in Table 5. This distribution includes the $2J + 1$ multiplicity of each J state due to the degeneracy of the m_j states under the experimental conditions, where m_j is the quantum number for that component of the angular momentum of the molecule along the axis of the rotation. However, since there is twice as much ortho- D_2 as para- D_2 in deuterium gas, the populations of the even states must be multiplied by two. These corrected relative populations are also given in Table 5.

Table 5. Relative Populations of the Lower Rotational Energy Levels of D_2 at 300°K

J	Relative Population	Corrected Relative Population
0	44.6	89.2
1	100.0	100.0
2	93.0	186.0
3	54.2	54.2
4	21.7	43.4
5	6.2	6.2
6	1.3	2.6
7	0.2	0.2

Relative transition probabilities were obtained by dividing the relative intensities of each transition by the corrected populations of the corresponding ground rotational levels and normalizing the sum of the probabilities for transitions observed at a given velocity to one. These probabilities for the system $Ar^+ + D_2$ in the relative energy range of 0.954-1.54 eV have been corrected for velocity discrimination by the detector aperture and are presented in Figure 10. The error bars, representing the reproducibility and expected uncertainty of each determination, are functions of peak shape and detector noise. It should be stressed that the rotational probabilities obtained in this work are relative probabilities and may be considered absolute only if no transitions above $J = 4 \rightarrow 6$ occur. Unfortunately, this requirement is difficult to verify experimentally. Due to the small weighting factors for transitions from levels greater than $J = 4$, a relatively insignificant hump in the high energy loss region of the velocity spectrum would

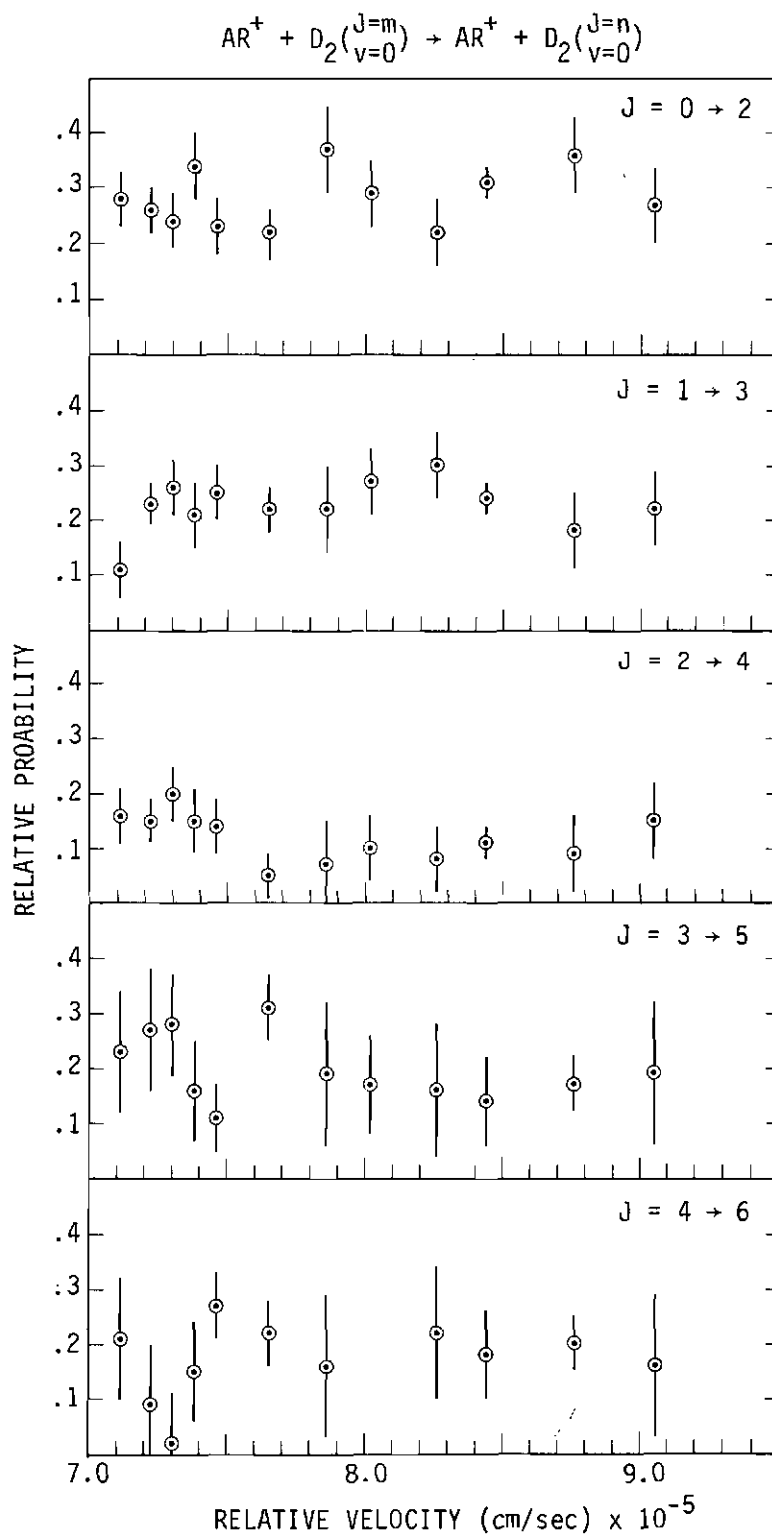


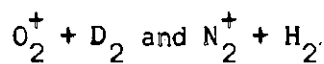
Figure 11. Variation in Relative Rotational Transition Probabilities with Relative Velocity in System $\text{Ar}^+ + \text{D}_2$.

correspond to a probability for a high J transition far greater than for $J = 0 \rightarrow 2$. The present apparatus cannot be expected to detect such transitions.

Differential inelastic cross sections for specific rotational transitions (σ) may be obtained from the ratio of the intensity of the inelastic peak (i_s) to that of the primary beam with no gas in the collision chamber (i_p), the path length over which a collision can occur (X), and the number density of the target molecules (n) along this path as related by the equation

$$\sigma = \frac{i_s}{nXi_p} . \quad (29)$$

While there has been no accurate pressure calibration of the present apparatus, the pressure in the scattering chamber may be estimated to within an order of magnitude knowing the pressure reduction in the static leak from the gas sample system and the pressure outside the collision chamber. The average differential inelastic cross section thus obtained for the $J = 0 \rightarrow 2$ transition is approximately $0.15 \pm 0.10 \text{ \AA}^2/\text{sr}$. This compares favorably with the value of $0.15 \text{ \AA}^2/\text{sr}$ observed by Bernstein (2) for the same transition in the system $K + D_2$.



Relative differential inelastic cross sections have also been measured for rotational excitation in the systems $O_2^+ + D_2$ and $N_2^+ + H_2$. The velocity spectra for these systems is somewhat complicated due to broadening of the peaks by rotational transitions of the incident ions occurring within the ion source and optics. This resulted in poor

resolution of peaks corresponding to rotational transitions of the target molecules with a subsequent loss of accuracy in the determination of their positions and intensities. The results for these systems are listed in Table 6 and should be considered to have error limits of ± 50 per cent associated with each value.

Table 6. Relative Transition Probabilities Normalized to the Sum of the Transition Probabilities Observed at a Given Velocity

System	Relative Velocity (cm/sec) $\times 10^{-5}$	Transition $J_m \rightarrow J_n$	Relative Transition Probabilities
$O_2^+ + D_2$	8.09	0 \rightarrow 2	0.44
		1 \rightarrow 3	0.19
		2 \rightarrow 4	0.06
		3 \rightarrow 5	0.16
		4 \rightarrow 6	0.15
	9.35	0 \rightarrow 2	0.12
		1 \rightarrow 3	0.18
		2 \rightarrow 4	0.11
		3 \rightarrow 5	0.18
		4 \rightarrow 6	0.41
$N_2^+ + H_2$	10.43	0 \rightarrow 2	0.42
		1 \rightarrow 3	0.03
		2 \rightarrow 4	0.48
		3 \rightarrow 5	0.03
		0 \rightarrow 4	0.04

Vibrational Excitation

General

Relative differential cross sections for the collisional excitation of specific vibrational transitions have been obtained for the

systems $O^+ + O_2$ and $N_2^+ + N_2$. The analysis of the velocity spectra was conducted the same as that for rotational excitation described in an earlier section. Vibrational transitions were observed as distinct humps on the velocity spectra of the forward scattered ions. However, subtraction of the velocity spectrum of the control systems using He as the target gas did not result in well shaped peaks in the inelastic spectrum, since rotational-vibrational bands rather than pure vibrational transitions are observed.

$O^+ + O_2$

The system $O^+ + O_2$ has been studied at energies of 9.9, 14.6, and 20.0 eV in the LAB system. The results observed with target gas in the collision chamber are shown in Figures 12, 13, and 14. The widths of the bars represent the uncertainty in measuring the energies of the peak maxima. The positions of these maxima predicted by the kinematics of the collision are shown at the top of the figures. The values of $\Delta\epsilon$ used in Equation (24) are the energy differences between the vibrational states of the harmonic oscillator

$$\Delta\epsilon = E(v=v, J=0) - E(v=0, J=0) = vhc\bar{\nu} \quad (30)$$

where v is the quantum number of the oscillator state, h is Planck's constant, c is the speed of light, and $\bar{\nu}$ is the frequency of the oscillator in units of wavenumbers (cm^{-1}). Values of $\bar{\nu}$ for most diatomic molecules are tabulated in Reference 18. For the particular case of O_2 , $\bar{\nu} = 1580.361 \text{ cm}^{-1}$ (18).

It can be seen from these data that the probability of multi-quantum transitions increases dramatically with increasing relative

POSSIBLE TRANSITIONS

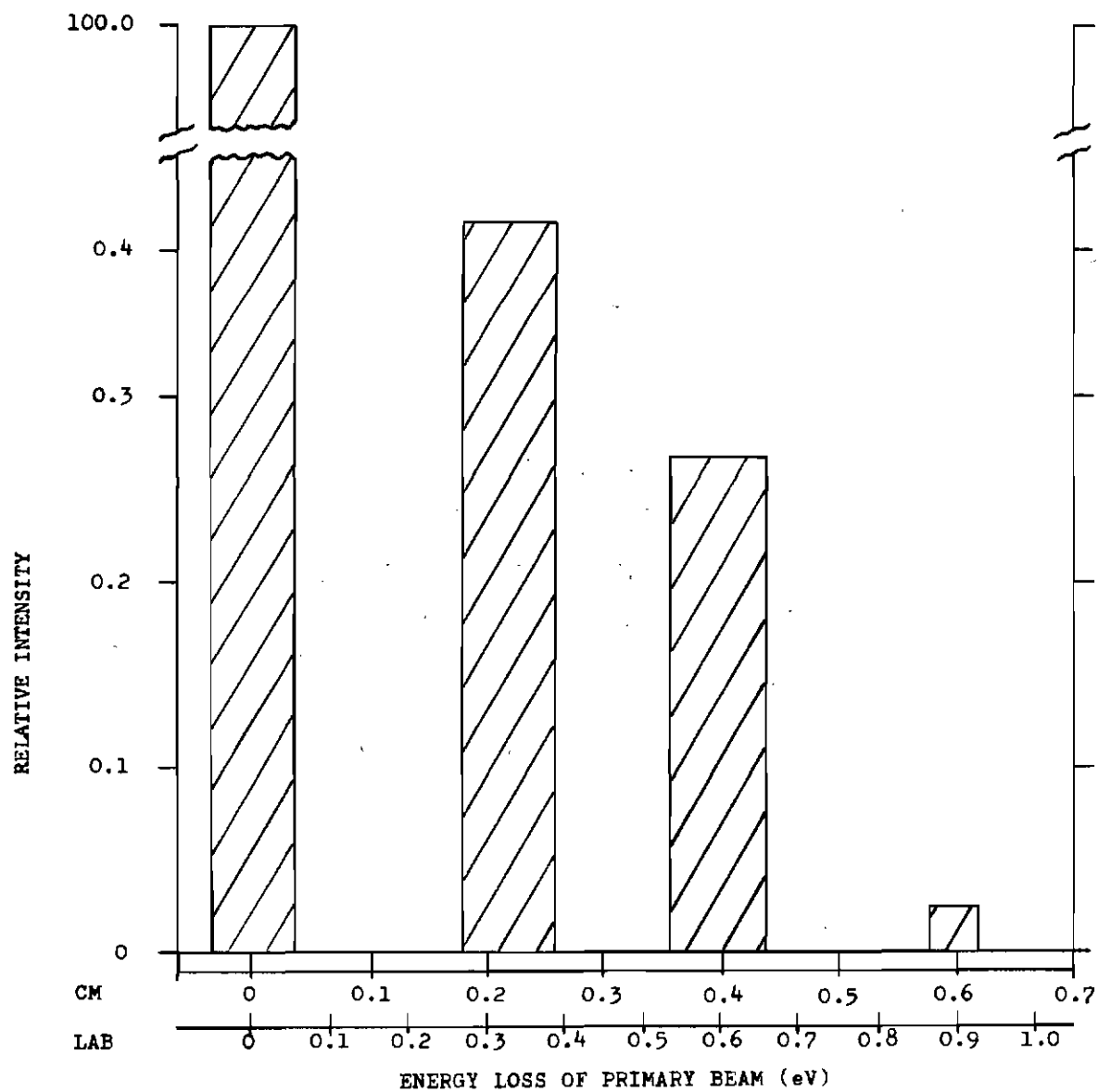
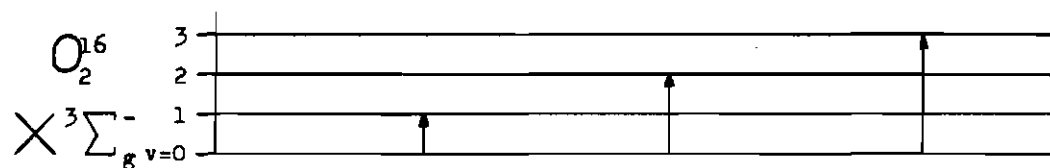


Figure 12. Energy Loss Spectrum of 9.9 eV LAB O^+ in System $O^+ + O_2$.

POSSIBLE TRANSITIONS

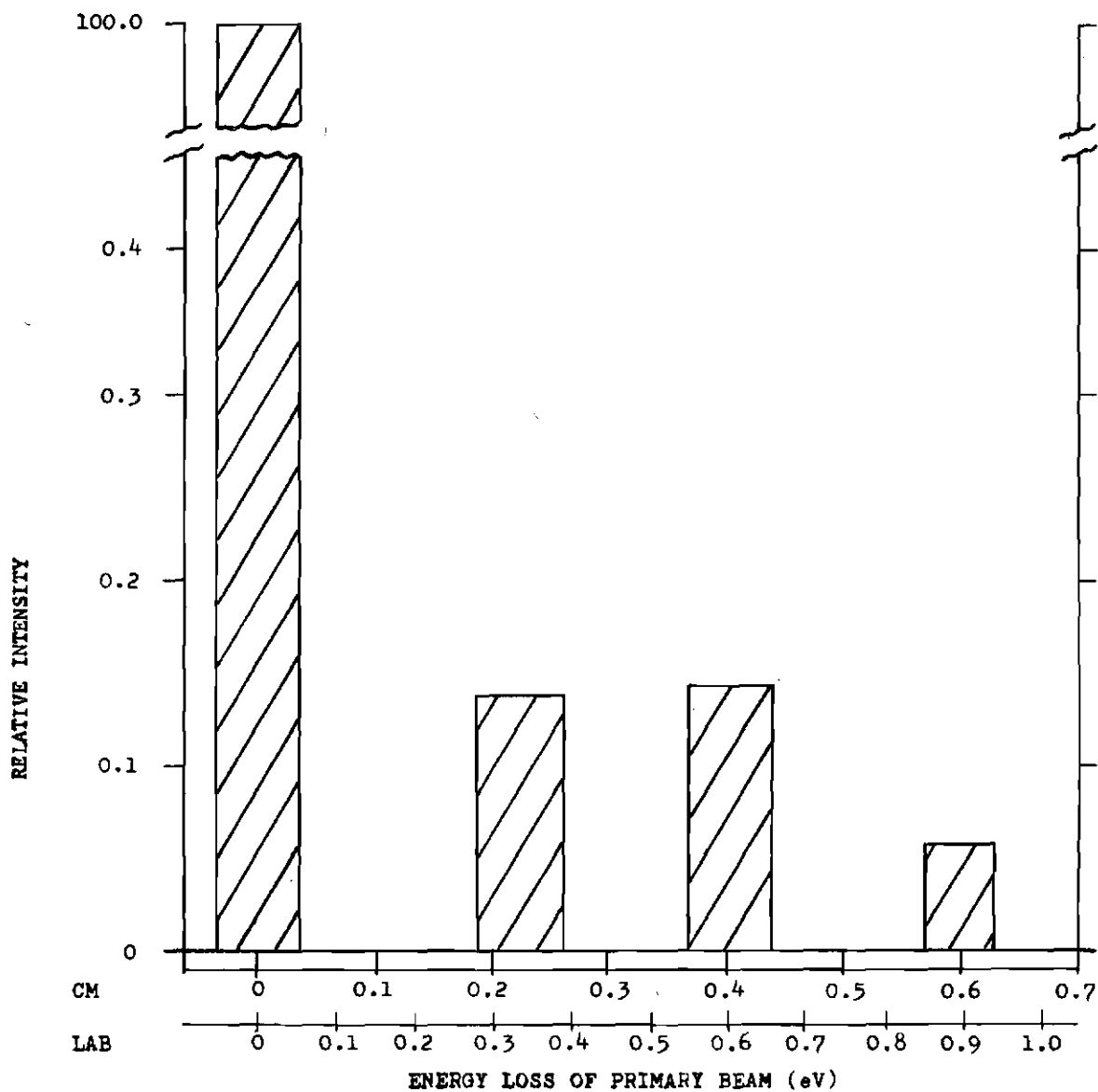
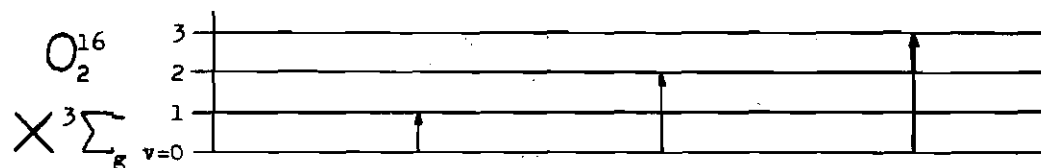


Figure 13. Energy Loss Spectrum of 14.6 eV LAB O^+ in System $O^+ + O_2$.

POSSIBLE TRANSITIONS

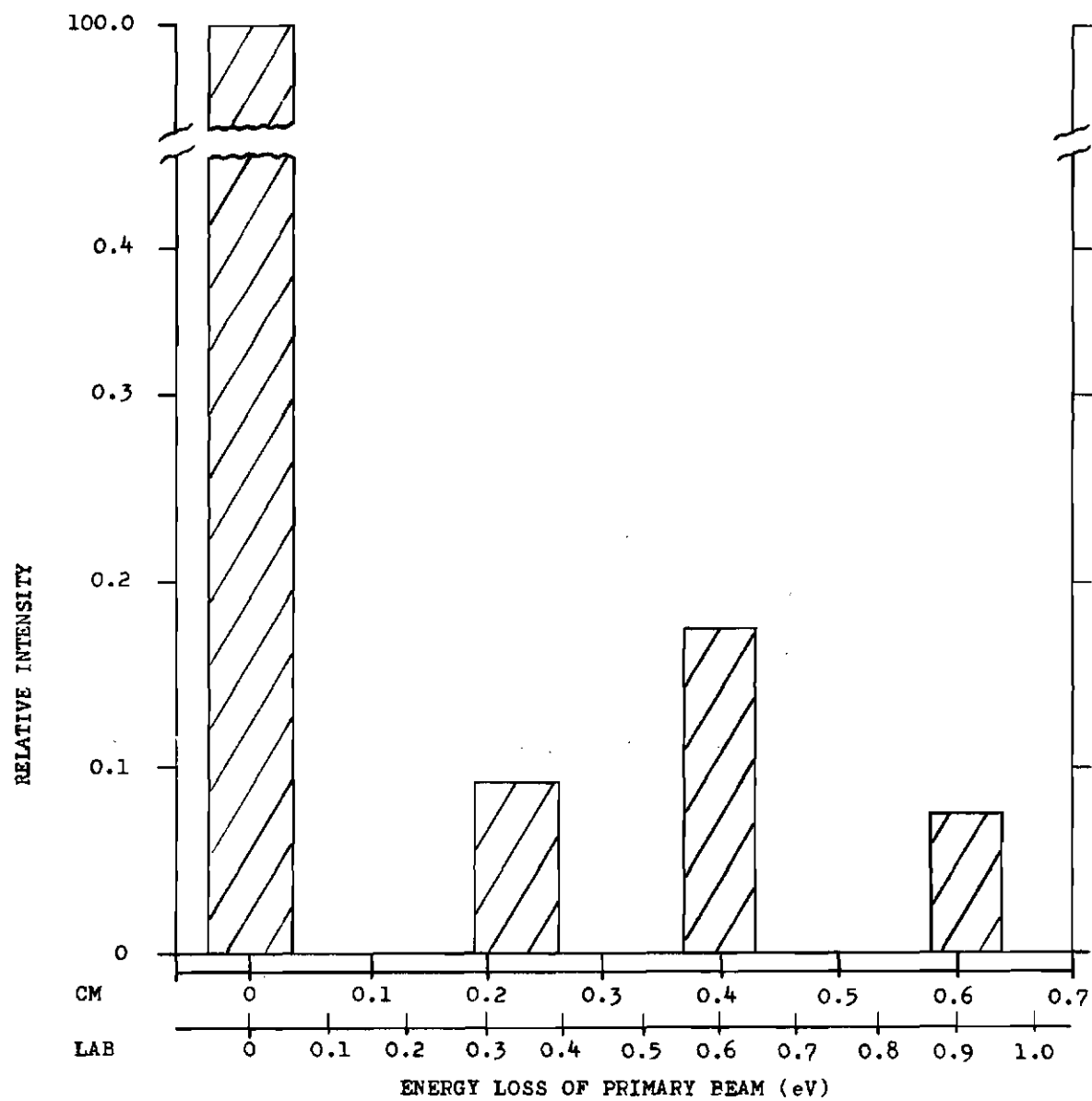
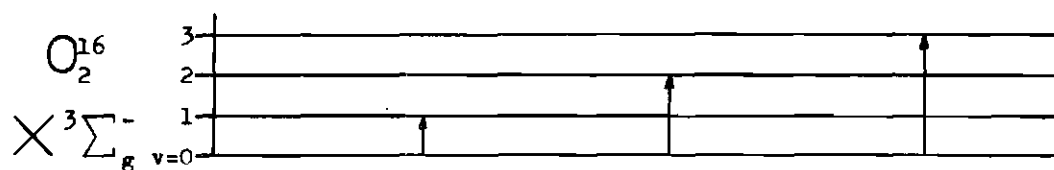


Figure 14. Energy Loss Spectrum of 20.0 eV LAB O^+ in System $O^+ + O_2$.

energy. A similar increase has been observed qualitatively by Schöttler and Toennies (3) in the system $\text{Li}^+ + \text{H}_2$. In the following chapter, the experimental transition probabilities for the system $\text{O}^+ + \text{O}_2$ will be compared with those predicted by theory.

$\text{N}_2^+ + \text{N}_2$

The system $\text{N}_2^+ + \text{N}_2$ has been studied at an energy of 15.6 eV in the LAB system. It has been extremely difficult to obtain a stable N_2^+ beam in the present apparatus. After only a short period of operation, nitrides formed at the surface of the filament cause fluctuations in the electron emission which, in time, lead to fluctuations in the intensity of the primary ion beam. For this reason, only one spectrum suitable for analysis has been obtained in this system. These results are presented in Figure 15.

It should be noted that vibrational excitation of either the incident ion or the target molecule, or simultaneous excitation of both is possible in this system. The vibrational frequencies of the ion and the molecule are quite similar. For N_2^+ , $\bar{\nu} = 2207.19 \text{ cm}^{-1}$ (18), while for N_2 , $\bar{\nu} = 2359.61 \text{ cm}^{-1}$ (18). This difference in the frequencies of the molecule and the ion cannot be resolved for the lower vibrational transitions, as may be seen in Figure 15. However, for transitions at the higher energy losses, the energy differences become more marked, until two peaks are finally resolved in the region of relative energy loss between 0.8 and 0.9 eV.

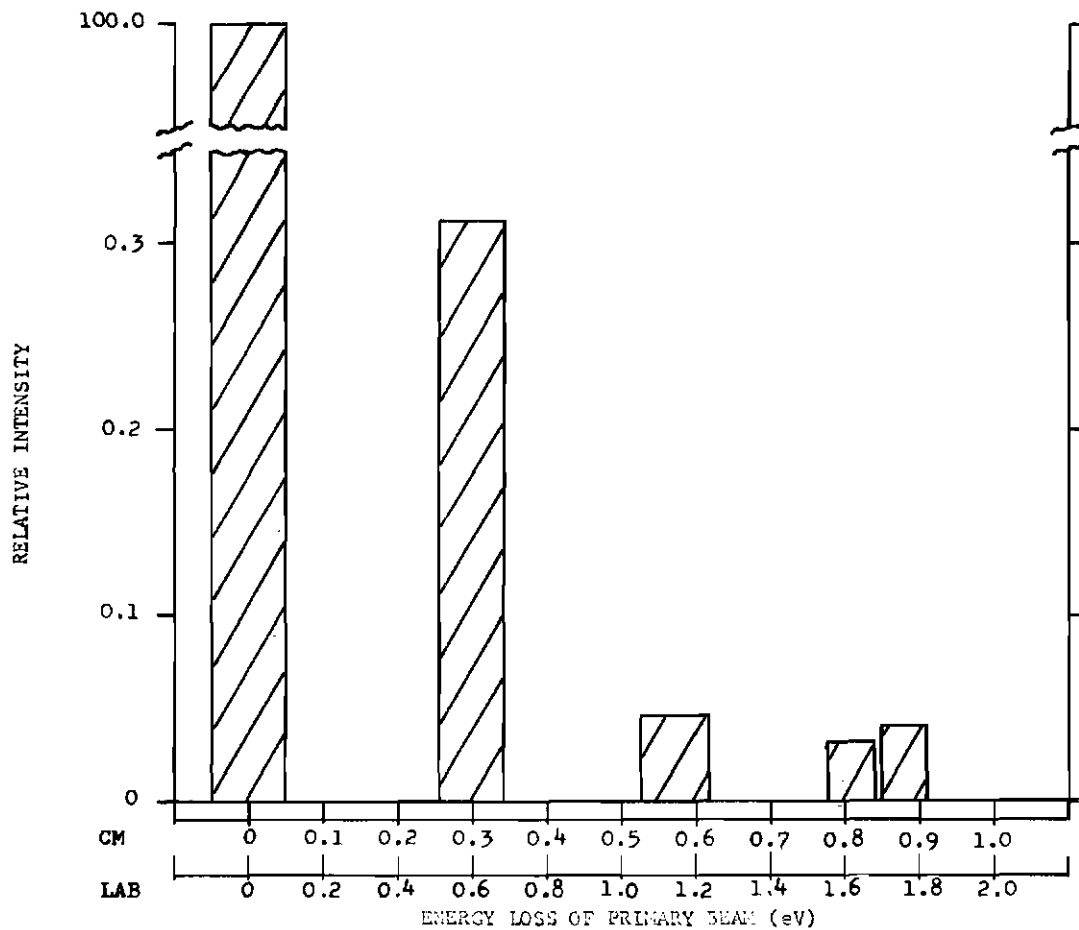
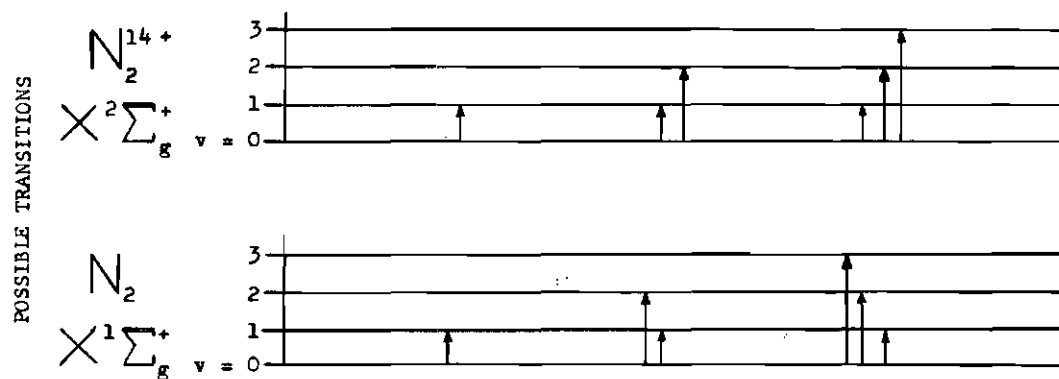


Figure 15. Energy Loss Spectrum of 15.6 eV LAB N_2^+ in System $N_2^+ + N_2$.

CHAPTER V

COMPARISON WITH THEORY

Introduction

In this chapter, the experimental results obtained for the collisional excitation of vibrational transitions in the system $O^+ + O_2$ will be compared with those predicted by theory for this system.

Indeed, much theoretical work has been done in the area of vibrational excitation.* Secrest and Johnson (6) have presented an exact quantum mechanical calculation for the collinear collision of a particle with a harmonic oscillator. An exponential interaction potential was used and transition probabilities were calculated for several different mass combinations of the particles. Somewhat earlier, Kelley and Wolfsberg (22) obtained transition probabilities for the same model using an exact classical calculation. Unfortunately no system approximating that of $O^+ + O_2$ was used in either of these calculations and both required extensive machine computation of the respective equations of motion, even for such a simple model.

For these reasons, the treatment which will be followed in this chapter is an approximate quantum-mechanical calculation developed by Kerner (23) and Treanor (1). This treatment leads to analytic solutions for a general class of interaction potentials. In addition, Treanor (1)

*For a review of theoretical work in this area before 1964, see Takayanagi (20), (21).

has shown the results of this approximate quantum-mechanical calculation reduce to those of a semiclassical calculation. For several systems, the relationship among the transition probabilities predicted by each of the three treatments is known* in order to approximately compare the experimental results with those which should be predicted by the exact quantum mechanical treatment.

Classical Calculation

Consider the collinear collision of a particle A incident along the bond axis of a diatomic molecule B_2 . Let x be the distance from the center of A to the center of mass of B_2 , y the internuclear distance of B_2 at any time t , y_0 the equilibrium internuclear distance of B_2 , $\tilde{m} = 2m_A m_B / m_A + 2m_B$ the reduced mass of the system, and $\mu = 1/2m_B$ the reduced mass of the molecule B_2 . To a first approximation, the interaction between A and the atom B further from it is much smaller than that between A and the closer B-atom and, therefore, may be neglected. The potential for the system can then be written as

$$V(x, y) = 1/2 k Y^2 - YF(t) \quad (31)$$

where $Y = y - y_0$, k is the harmonic oscillator force constant, and $F(t)$ is the classical force acting on the closer B-atom due to the collision with A.

The time-dependent Schrödinger equation for this system may be written as

* A comparison of these theories and others may be found in the recent review by Rapp (24).

$$-\frac{\hbar^2}{4} \frac{\partial^2 \psi}{\partial Y^2} + [1/2 k Y^2 - Y F(t)] = i \hbar \frac{\partial \psi}{\partial t} \quad (32)$$

Kerner (23) has obtained a solution to this equation via the transformations

$$\psi(Y, t) = \phi[Y - u(t), t] \exp[Y g(t)] \quad (33)$$

$$\xi(Y, t) = Y - u(t)$$

where $g(t)$ and $\phi(\xi, t)$ are undetermined functions. g and u are chosen such that Equation (32) is separable in the variables ξ and t with the solution

$$\psi_m(Y, t) = N_m \exp\left(\frac{i}{\hbar} \mu Y \dot{u}\right) \exp\left(-\frac{i}{\hbar} \int_0^t (\delta + E_n) dt\right) \cdot \quad (34)$$

$$\exp\left[-1/2 \alpha^2 (Y - u)^2\right] H_m[\alpha(Y - u)]$$

where $\delta = 1/4 \mu \dot{u}^2 - 1/2 k u^2$, N_m is a normalization factor $[\alpha/(\pi)^{1/2} 2^n n!]^{1/2}$, $\alpha^2 = (\mu k)^{1/2}/\hbar$, H_m is the m th Hermite polynomial, and $E_m = (m + 1/2)\hbar\omega$ is the energy of the m th vibrational state of the harmonic oscillator.

This solution may be interpreted (23) as describing an oscillating wave packet whose center moves under the equations of motion of the classical forced oscillator

$$\mu \ddot{u} + k u = F(t) \quad (35)$$

Following the procedure of Treanor (1), the wave function for the forced oscillator in the vibrational state m , $\psi_m(Y, t)$, may be expanded in terms of the complete set of normalized harmonic oscillator wave functions

$$X_n(Y, t) = N_n \exp(-1/2 \alpha^2 Y^2) H_n(\alpha Y) \exp(-i E_n t / \hbar) \quad (36)$$

such that

$$\psi_m(Y, t) = \sum_0^\infty b_{mn}(t) X_n(Y, t) \quad (37)$$

Hence

$$b_{mn} = \int_{-\infty}^t X_n \psi_m dt \quad (38)$$

where the course of the collision occurs in the interval $t = -\infty$, $x = \infty \rightarrow t = \infty$, $x = \infty$. Using Equations (34) and (36), Treanor (1) has integrated equation (38) to obtain

$$b_{mn} = (-1)^m (m! n!)^{1/2} \exp(-1/2 \epsilon_0) S_{mn} \epsilon_0^{(m+n)/2} \quad (39)$$

$$\exp[-i(m-n)(\omega t + \theta_t) - \frac{i}{\hbar} \left(\int_{-\infty}^t \delta dt - \mu \frac{\dot{u}u}{2} \right)]$$

where

$$S_{mn} = \sum_{j=0}^z \frac{(-1)^j \epsilon_0^{-j}}{(n-j)! j! (m-j)!} \quad (40)$$

$$\theta = \tan^{-1} (\dot{u}/\omega u), \quad (41)$$

z is the lesser of m and n , $\omega = 2\pi\nu$ is the angular frequency of the oscillator, and

$$\epsilon_0(t) = (1/4 \dot{u}^2 + 1/2 k u^2) / \hbar \omega \quad (42)$$

It can be seen that ϵ_0 is simply the total energy transferred to the classical forced oscillator divided by $\hbar\omega$, and will be written

$$\epsilon_0 = \frac{\Delta E_c}{\hbar\omega}. \quad (43)$$

If the oscillator is in the state m at $t = -\infty$, the probability of finding it in the state n at time t is then the square of the magnitude of the expansion coefficient b_{mn}

$$P_{mn} = |b_{mn}|^2 = m!n! e^{-\epsilon_0} \epsilon_0^{m+n} S_{mn}^2, \quad (44)$$

or for the particular case of $m = 0$

$$P_{on} = (1/n!) e^{-\epsilon_0} \epsilon_0^n. \quad (45)$$

As Rapp (25) has pointed out, this probability function of Treanor rises to a maximum transition probability at $\epsilon_0 = n$ with increasing relative energy of the collision and then decreases with a further increase in the relative energy.

To calculate the transition probabilities for a particular system, one must find the classical energy transferred to the oscillator in the collision. This energy is proportional to the square of the vibrational amplitude Y . Hence Y must be determined from the classical equation of motion of the oscillator as a function of the impulse $F(t)\delta t$. This problem has already been solved for a general class of oscillators (26). For the particular case of the undamped, forced oscillator

$$Y = \int_{-\infty}^{t'} \frac{F(t)}{\mu\omega} e^{i\omega t} dt \quad (46)$$

The classical energy transferred to the oscillator during the course of the collision is then (26)

$$\Delta E_c = \frac{1}{2\mu} \left| \int_{-\infty}^{\infty} F(t) e^{i\omega t} dt \right|^2. \quad (47)$$

A suitable potential function must now be found which will provide an accurate description of the interaction for a given physical system and yet yield solutions to Equation (47) in closed form. Two potentials that fit this latter requirement are available. Unfortunately, the first requirement may be only approximated.

Rapp (27) has proposed an exponentially repulsive potential of the form

$$V_L(X, Y) = E_0 \exp(-X/L) \exp(1/2 Y/L) \quad (48)$$

where $E_0 = 1/2 \tilde{m} v_0^2$ is the total energy of the system and $X = x - x_{\min}$, where x_{\min} is the value of x at the time of collision (classical turning point). L is a parameter used to fit an exponential potential to the repulsive slope of the Lennard-Jones potential function* and may be interpreted as the effective range of the interaction. If the potential is only weakly dependent on the vibrational amplitude, that is if $Y \ll L$, then the exponential may be expanded in terms of Y to obtain

* See Appendix.

$$V_I(X, Y) = E_0 \exp(-X/L)(1 - 1/2 Y/L) . \quad (49)$$

To a first approximation, the trajectory of particle A may be considered independent of Y

$$V_I(X) \cong E_0 \exp(-X/L) \quad (50)$$

and this approximate potential substituted into the equation of motion of A

$$1/2 \tilde{m} \dot{X}^2 = E_0 - V_I(X) . \quad (51)$$

Rapp (26) has integrated Equation (51) to obtain

$$\exp(-X/L) = \operatorname{sech}^2(v_0 t/2L) . \quad (52)$$

Substitution of Equation (52) into Equation (49) yields

$$V_I(Y, t) = E_0 (1 + 1/2 Y/L) \operatorname{sech}^2(v_0 t/2L) . \quad (53)$$

The force of the interaction may now be calculated from $V_I(Y, t)$

$$F_I(t) = - \frac{\partial}{\partial Y} [V_I(Y, t)] = \frac{E_0}{2L} \operatorname{sech}^2(v_0 t/2L) . \quad (54)$$

Equation (47) has been solved by Rapp (27) for this force to obtain

$$\Delta E_{cI} = \frac{1}{24} [\pi \tilde{m} \omega L / \sinh(\pi \omega L / v_0)]^2 . \quad (55)$$

Hence the probability of the vibrational transition $v=0 \rightarrow n$ occurring in the collision is

$$P_{on} = \left(\frac{1}{n!}\right) e^{-\epsilon_o} \epsilon_o^n \quad (45)$$

where

$$\epsilon_o = \frac{2\pi^2 c \bar{\nu}}{h\mu} [\pi \tilde{m} L / \sinh(2\pi^2 c \bar{\nu} L / v_o)]^2, \quad (56)$$

c is the speed of light, and $\bar{\nu}$ is the frequency of the oscillator in units of cm^{-1} . A plot of equations (45) and (56) for the system $O^+ + O_2$ versus relative velocity for three values of L is shown in Figure 16.

Here $m_A = m_B = 2.66 \times 10^{-23} \text{g}$ and $\bar{\nu} = 1580.36 \text{ cm}^{-1}$ (18).

Kelley and Wolfsberg (22) have pointed out that this potential does not permit energy conservation in high energy collisions for certain mass combinations in the collision system. Consider the high energy limit of the classical energy transferred to the oscillator

$$\lim_{v_o \rightarrow \infty} E_{cI} = \frac{\tilde{m}}{\mu} E_o. \quad (57)$$

For the case of $O^+ + O_2$, the factor \tilde{m}/μ is on the order of 2.7. Hence, energy is not conserved by this potential in the system of interest.

A second potential has been proposed by Rapp and Sharp (28) of the form

$$V_{II}(X, Y) = E_o \text{csch}^2[(X/8L) + \rho] \exp(Y/21) \quad (58)$$

where ρ is a constant whose value is such that $\text{csch}^2 \rho = 1$. This potential has been obtained as a function of the oscillator amplitude and time in a manner analogous to that used for V_I (28).

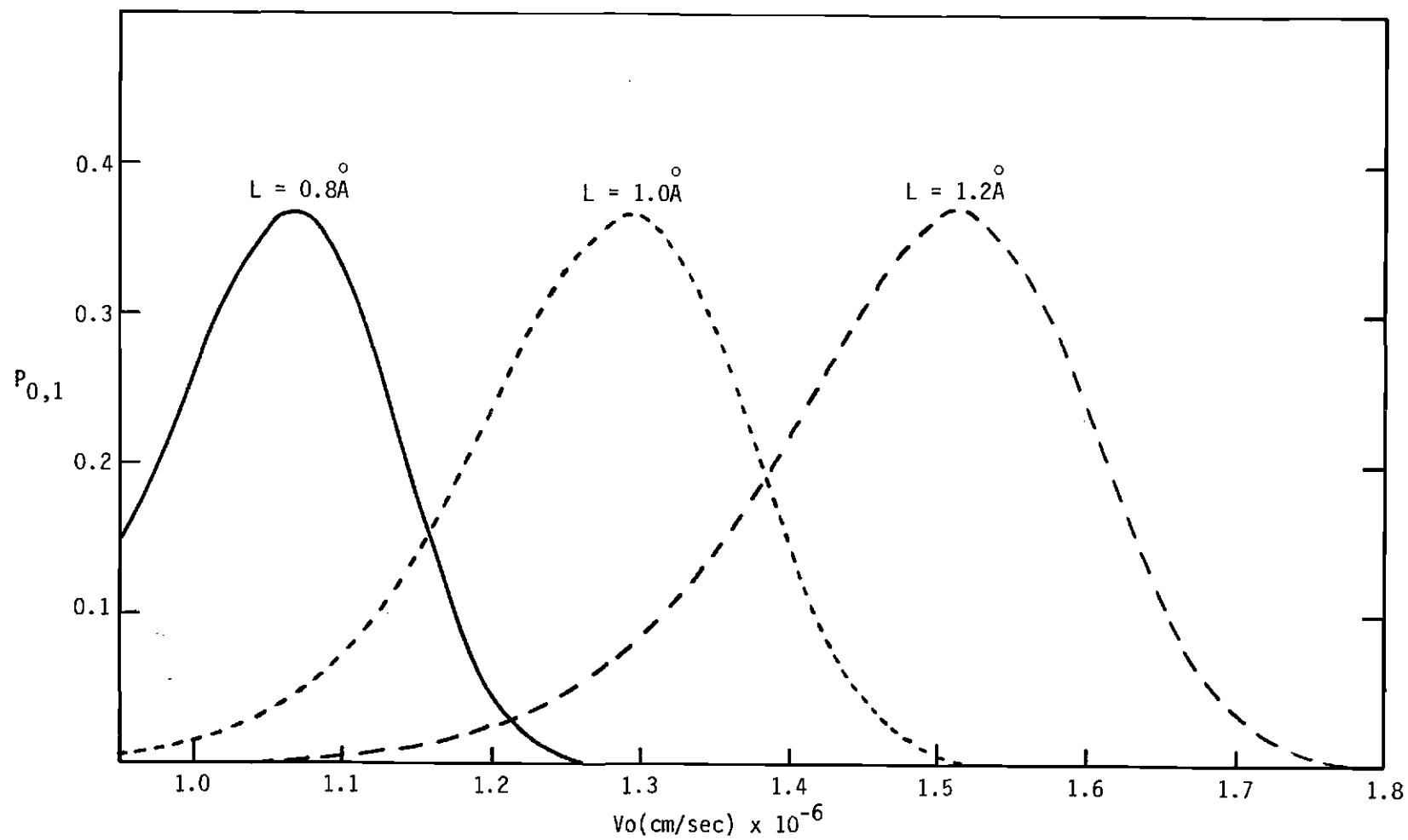


Figure 16. Variation with L of Vibrational Transition Probabilities Calculated from Equations (45) and (56) for the System $\text{O}^+ + \text{O}_2$.

$$V_{II}(Y, t) = E_0 \exp(Y/2L) \operatorname{sech}(\pi v_0 t/4L) \quad (59)$$

or equivalently

$$F_{II}(t) = -(E_0/2L) \exp(Y/2L) \operatorname{sech}(\pi v_0 t/4L) . \quad (60)$$

If $Y \ll L$, Equation (60) may be expanded in terms of Y to obtain

$$F_{II}(t) = -(E_0/2L) \operatorname{sech}(\pi v_0 t/4L) . \quad (61)$$

Treanor (1) has integrated Equation (47) for this force to obtain the classical energy transferred to the oscillator

$$E_{cII} = \frac{\tilde{m}^2 v_0^2}{\mu} \operatorname{sech}^2(2\omega L/v_0) . \quad (62)$$

Equation (45) may be used to calculate the transition probabilities, where ϵ_0 is given by

$$\epsilon_0 = \frac{\tilde{m}^2 v_0^2}{\mu h c \tilde{\nu}} \operatorname{sech}^2(4\pi c \tilde{\nu} L/v_0) . \quad (63)$$

P_{01} for the system $O^+ + O_2$ using this potential is plotted versus the relative velocity of the collision for three values of L in Figure 17.

Comparison of Results

The probabilities for the vibrational transitions $v = 0 \rightarrow 1$, $v = 0 \rightarrow 2$, and $v = 0 \rightarrow 3$ predicted for the system $O^+ + O_2$ by Equations (45) and (63) are shown in Figures 18-20. Also shown are the experimental transition probabilities for this system whose sum at each

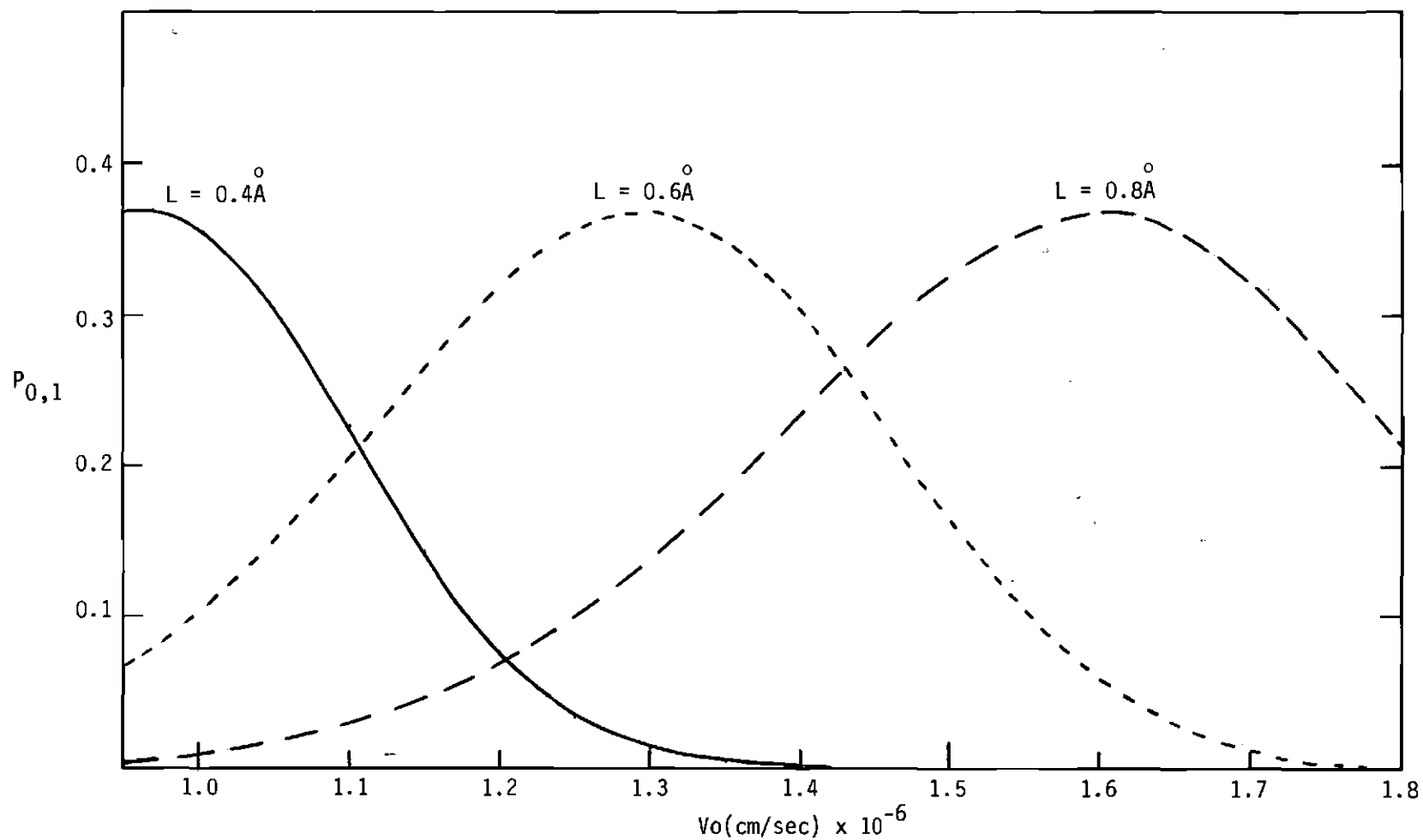


Figure 17. Variation with L of Vibrational Transition Probabilities Calculated from Equations (45) and (63) for the System $0^+ + 0_2$.

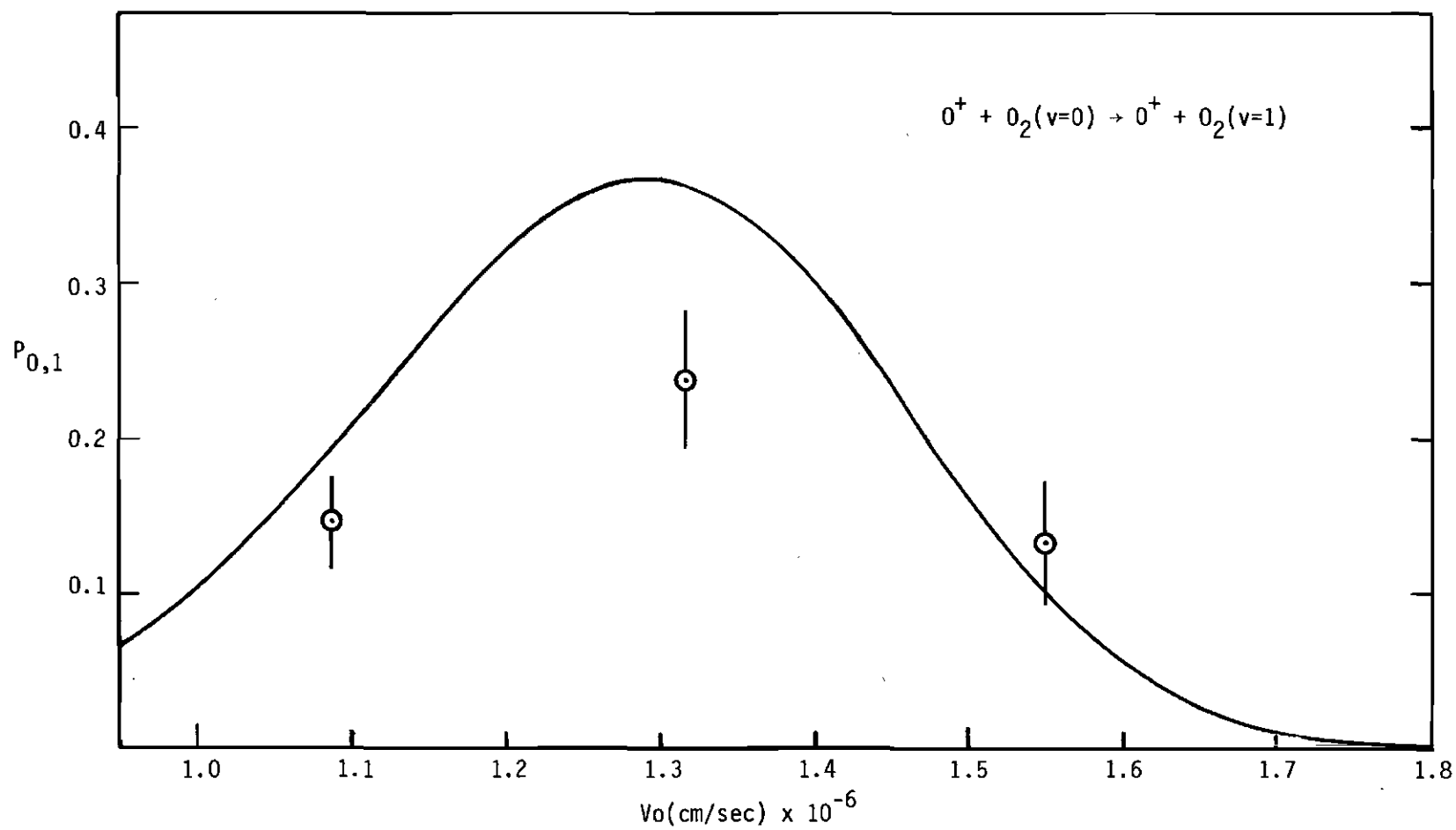


Figure 18. Probability of the Transition $v = 0 \rightarrow 1$ in the System $O^+ + O_2$ Compared to That Predicted by Equations (45) and (63). $L = 0.600 \text{ \AA}$.

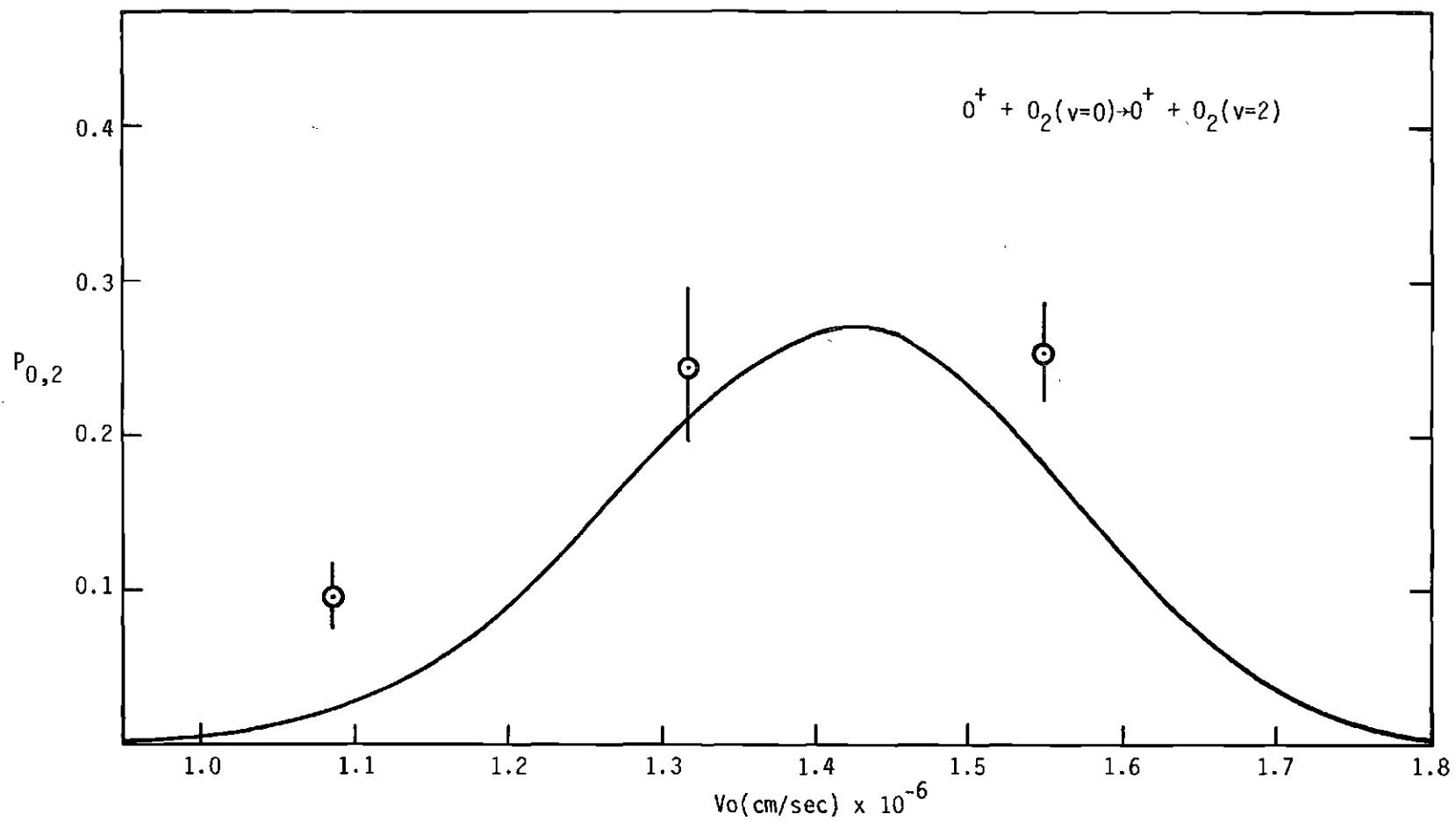


Figure 19. Probability of the Transition $v = 0 \rightarrow 2$ in the System $0^+ + O_2$ Compared to That Predicted by Equations (45) and (63). $L = 0.600 \text{ \AA}$.

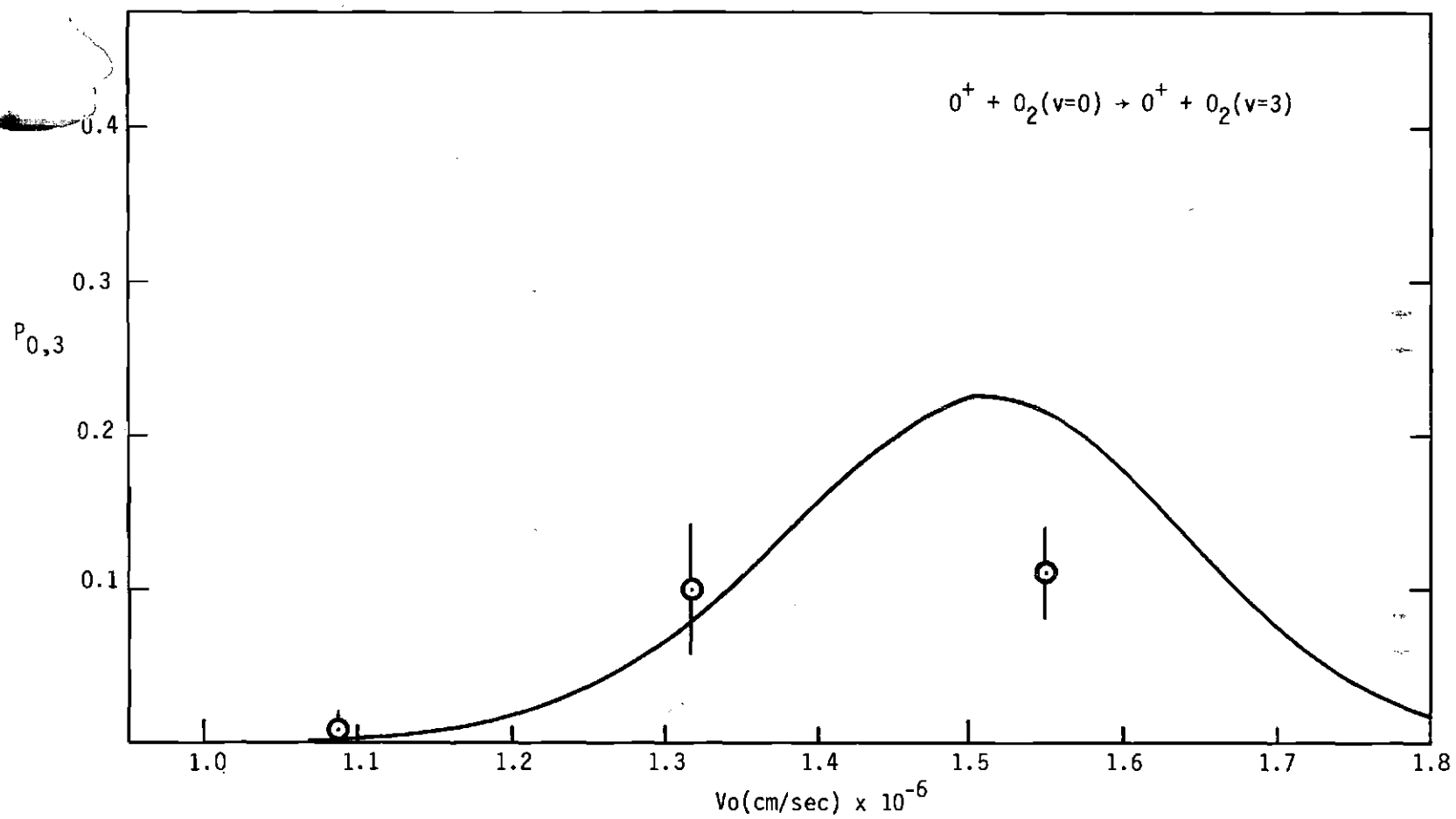


Figure 20. Probability of the Transition $v = 0 \rightarrow 3$ in the System $O^+ + O_2$ Compared to That Predicted by Equations (45) and (63). $L = 0.600 \text{ \AA}$.

velocity has been normalized to the sum predicted by theory at the same velocity. To fit the theoretical curves to the data, a value of $L = 0.600$ Å had to be chosen. However, for collisions in the system $O_2 + O_{2'}$ the value of this parameter is normally on the order of 0.26 Å (29). Parker (29) has obtained an empirical expression for calculating L from the Lennard-Jones molecular diameter r_0 which fits his experimental data

$$\alpha = 2.625 \left\{ 1 - \exp[-(r_0/3.46)^6] \right\} \quad (64)$$

$$+ 6.117 (r_0/3.46)^6 \exp[-(r_0/3.46)^6]$$

where $\alpha \approx L^{-1}$. In the region below $\alpha = 4.0$ ($L = 0.25$) L increases monotonically with decreasing r_0 . Hence, the larger value of L required to fit the data implies a smaller equilibrium internuclear distance between the incident particle and the diatomic molecule.

The presence of this observed decrease in r_0 is readily explained in part by recalling the incident particle is charged. Therefore an additional potential due to polarization of the molecule by the incident ion must be considered. Such a polarization appears in the Lennard-Jones potential function as an additional term proportional to r^{-4} . This term effectively deepens the attractive potential well and shifts the equilibrium distance to smaller values of r_0 . Hence a larger value of L should be expected in this system than in that for a purely intermolecular collision.

Of course, part of the observed increase in the value of L is a form of compensation for approximations made in obtaining a computationally suitable potential and, indeed, in the model on which the

theory itself is based.

Kelley and Wolfsberg (22) have calculated the exact classical energy transferred in the collision (ΔE) for a large number of different mass combinations. They have found that the ratio of ΔE to that calculated assuming the coordinates X and Y are independent (ΔE_c) depends primarily on a mass ratio of the system. Rapp (25) has fitted their results to an empirical function to obtain

$$\frac{\Delta E_c}{\Delta E} = e^{1.685m} \quad (65)$$

where m for the case of a homonuclear diatomic molecule is given by $m = \tilde{m}/4\mu$. For the system $O^+ + O_2$, $m = 0.324$ and $\Delta E_c/\Delta E = 1.75$. The maximum probability calculated from Equation (45) for the $v = 0 \rightarrow 1$ transition will therefore be only 0.304 that which would have been obtained if ΔE had been used in the calculation. This difference appears as an additional shift to higher values of L as may be seen from the L dependence of the probability function shown in Figure 17.

Secrest and Johnson (6) have compared their exact quantum mechanical results to those of Kelley and Wolfsberg (21) for a number of systems. In the case most analogous to that of $O^+ + O_2$, the exact quantum transition probabilities were found to be somewhat lower than those predicted by the exact classical theory. The comparison, however, was made on the ascending branch of the P_{On} versus v_o curve, hence L must be increased still further to approximate the quantum results.

It may be seen that the experimental data for the system

$O^+ + O_2$ fits the vibrational transition probabilities predicted by the theory of Kerner (23) and Treanor (1) surprisingly well. However some of this correspondence may only be fortuitous considering the crudeness of the model on which this theory is based.

CHAPTER VI

CONCLUSIONS

An ion beam technique has been utilized to measure relative differential inelastic cross sections of specific rotational and vibrational transitions in diatomic molecules due to collisional excitation. The technique consists of passing a low energy, mass selected ion beam through a rotatable collision chamber containing the target gas. The inelastically scattered ions are mass selected and velocity analysed. The excitation of specific transitions appears as discrete peaks in the velocity spectrum of the forward scattered ions.

The variation in the differential inelastic cross sections for rotational excitation with the relative velocity of the collision partners has been studied in detail for the system $\text{Ar}^+ + \text{D}_2$. These results are presented in Figure 11. Transitions other than $\Delta J = +2$ have not been observed. The absolute differential cross section for the excitation of the $J = 0 \rightarrow 2$ rotational transition in D_2 is estimated to be $0.15 \pm 0.10 \text{ \AA}^2/\text{sr}$, which is in good agreement with the value obtained by Bernstein (5) in the system $\text{K} + \text{D}_2$. Relative differential inelastic cross sections have also been obtained in the systems $\text{O}^+ + \text{D}_2$ and $\text{N}_2^+ + \text{H}_2$.

The velocity dependence of the probability for the vibrational transitions $v = 0 \rightarrow 1$, $v = 0 \rightarrow 2$, and $v = 0 \rightarrow 3$ has been studied in the system $\text{O}^+ + \text{O}_2$. It is observed that the most probable vibrational

transitions at low kinetic energy of impact involve a change in vibrational quantum number of unity; however, at higher relative energies multiquantum transitions predominate. These results have been compared with the transition probabilities predicted for this system by the approximate quantum-mechanical theory developed by Kerner (23) and Treanor (1) for the collinear collision of a particle with a harmonic oscillator. Inaccuracies in the theory and in the interaction potential may be approximately corrected by a variation in the potential parameter L . Surprisingly good agreement is achieved between experiment and theory.

APPENDIX

SIGNIFICANCE OF PARAMETER L

Herzfeld (30) has presented a method for fitting a simple exponential potential to the intermolecular Lennard-Jones (LJ) potential function

$$V = 4\beta[(r_0/r)^{12} - (r_0/r)^6] \quad (A-1)$$

The r^{-6} term is simply the potential due to the long range London attraction between molecules and the r^{-12} term is an approximation of the short range intermolecular repulsion due to overlapping of electron orbitals of the molecules. β is a parameter chosen to represent the depth of the potential well and r_0 is the internuclear distance at which $V = 0$. The equilibrium internuclear distance for the system, that is the value of r at which V is a minimum, occurs at $r = 2^{1/6} r_0$.

Another term, r_c , must be defined before an exponential potential may be fitted to Equation (A-1) for the case of intermolecular collisions. Consider a particle A of total energy E incident on a second particle B. If the interaction between these particles may be represented by the LJ potential, the forward motion of A will be stopped by the repulsive part of the potential curve at a distance r_c from particle B.

Choose the exponential potential to be of the form

$$V' = V_0 e^{-r/L} - \beta \quad (A-2)$$

LITERATURE CITED*

1. Charles E. Treanor, J. Chem. Phys. 43, 532 (1965).
2. Anthony R. Blythe, Arthur E. Grosser, and Richard B. Bernstein, J. Chem. Phys. 41, 1917 (1964).
3. J. Schöttler and J. P. Toennies, Z. Physik 214, 472 (1968).
4. Roy G. Gordon, William Klemperer, and Jeffrey I. Steinfeld, Ann. Rev. Phys. Chem. 19, 215 (1968).
5. Peter F. Dittner and Sheldon Datz, J. Chem. Phys. 49, 1969 (1968).
6. Don Secrest and B. Robert Johnson, J. Chem. Phys. 45, 4556 (1966).
7. J. P. Toennies, Z. Physik 182, 257 (1965).
8. H. Pauly and J. P. Toennies, Advances in Atomic and Molecular Physics 1, 195 (1965).
9. A. O. Nier, Rev. Sci. Instr. 11, 212 (1940).
10. Jean H. Futrell and C. D. Miller, Rev. Sci. Instr. 37, 1521 (1966).
11. Hermann Wollnik, "Electrostatic Prisms," Focusing of Charged Particles, Vol. II. Edited by Albert Septier. New York: Academic Press, 1967.
12. A. L. Hughes and V. Rojansky, Phys. Rev. 34, 284 (1929).
13. A. L. Hughes and J. H. McMillen, Phys. Rev. 34, 291 (1929).
14. F. H. Field and J. L. Franklin, Electron Impact Phenomena. New York: Academic Press, 1957. p. 244.
15. Von A. Henglein, K. Lacmann, and G. Jacobs, Ber. Bunsenges. Physik. Chem. 69, 279 (1965).
16. Earl W. McDaniel, Collision Phenomena in Ionized Gases. New York: John Wiley and Sons, Inc., 1964. p. 7.

*The abbreviations used herein conform to those adopted by the IUPAC and AIP as described in the List of Periodicals, Chem. Abstr. 55, 1J (1961) and later supplements.

17. Herbert Goldstein, Classical Mechanics. Reading, Mass.: Addison-Wesley Publishing Company, Inc., 1950. p. 87.
18. G. Herzberg, Spectra of Diatomic Molecules. Vol. I: Molecular Spectra and Molecular Structure. 2d ed. Princeton, N. J.: D. Van Nostrand Company, Inc., 1950.
19. Norman Davidson, Statistical Mechanics. New York: McGraw-Hill Book Company, Inc., 1962. pp. 134 and 135.
20. Kazuo Takayanagi, Progr. Theoret. Phys. (Kyoto), Suppl. No. 25, 1 (1963).
21. Kazuo Takayanagi, Advances in Atomic and Molecular Physics 1, 149 (1965).
22. J. Daniel Kelley and Max Wolfsberg, J. Chem. Phys. 44, 324 (1966).
23. Edward H. Kerner, Can. J. Phys. 36, 371 (1957).
24. D. Rapp and T. Kassal, Chem. Rev. 69, 61 (1969).
25. D. Rapp and T. Kassal, A Review of the Theory of Vibrational Energy Transfer between Simple Molecules in Nonreactive Collisions. A Report Prepared by the Grumman Research Department. Bethpage, New York: Grumman Aircraft Engineering Corporation, 1968.
26. John C. Slater and Nathaniel H. Frank, Mechanics. New York: McGraw-Hill Book Company, Inc., 1947. pp. 37 and 38.
27. Donald Rapp, J. Chem. Phys. 32, 735 (1960).
28. D. Rapp and T. E. Sharp, J. Chem. Phys. 38, 2641 (1963).
29. J. G. Parker, J. Chem. Phys. 41, 1600 (1964).
30. Karl F. Herzfeld and Theodore A. Litovitz, Absorption and Dispersion of Ultrasonic Waves. New York: Academic Press, 1959. pp. 278-281.
31. Karl F. Herzfeld, "Relaxation Phenomena in Gases," Thermodynamics and Physics of Matter, Vol. I. Edited by F. D. Rossini. Princeton, New Jersey: Princeton University Press, 1955.